Journal of Materials Chemistry

Cite this: *J. Mater. Chem.*, 2011, **21**, 11686

www.rsc.org/materials

FEATURE ARTICLE

Mesoporous titania photocatalysts: preparation, characterization and reaction mechanisms

Adel A. Ismail*[a] and Detlef W. Bahnemann[b]

Received 26th January 2011, Accepted 6th May 2011
DOI: 10.1039/c1jm10407a

Titanium dioxide is a very important semiconductor with a high potential for applications in photocatalysis, solar cells, photochromism, sensoring, and various other areas of nanotechnology. Increasing attention has recently been focused on the simultaneous achievement of high bulk crystallinity and the formation of ordered mesoporous TiO_2 frameworks with high thermal stability. Mesoporous TiO_2 has continued to be highly active in photocatalytic applications because it is beneficial for promoting the diffusion of reactants and products, as well as for enhancing the photocatalytic activity by facilitating access to the reactive sites on the surface of photocatalyst. This steady progress has demonstrated that mesoporous TiO_2 nanoparticles are playing and will continue to play an important role in the protection of the environment and in the search for renewable and clean energy technologies. This review focuses on the preparation and characterisation of mesoporous titania, noble metals nanoparticles, transition metal ions, non-metal/doped mesoporous titania networks. The photocatalytic activity of mesoporous titania materials upon visible and UV illumination will be reviewed, summarized and discussed, in particular, concerning the influence of preparation and solid-state properties of the materials. Reaction mechanisms that are being discussed to explain these effects will be presented and critically evaluated.

[a]*Advanced Materials Department, Central Metallurgical R& D Institute, CMRDI, P.O. Box 87, Helwan, 11421, Cairo, Egypt. E-mail: aismail@cmrdi.sci.eg; Fax: +202-25010639; Tel: +202-25010643*

[b]*Institut für Technische Chemie, Leibniz Universität Hannover, Callinstrasse 3, 30167 Hannover, Germany*

Adel A. Ismail

Dr. Adel A. Ismail is Head of Nanostructured Materials & Nanotechnology Division, Central Metallurgical Research and Development Institute, Cairo, Egypt. He received his PhD degree in Chemistry from Ain Shams University in 2001, Cairo, Egypt. Ismail carried out postdoctoral research at University of Florida at Material Science department, USA (2003), National Institute of Advanced Industrial Science & Technology, Sendai, Japan (2005–2007), and Photocatalysis and Nanotechnology Research Unit at the Institute of Technical Chemistry of the Leibniz University Hannover (2008–2010). His research interests include sol–gel chemistry, design development porous photocatalysts and photocatalytic applications in destruction of organic compounds, hydrogen production and self-cleaning.

Detlef W. Bahnemann

Prof. Detlef W. Bahnemann has been Head of the Photocatalysis and Nanotechnology Research Unit at the Institute of Technical Chemistry of the Leibniz University Hannover since 2002. In the same year he was appointed as Honorary Professor of the Robert Gordon University in Aberdeen, UK. His research interests include photocatalysis, photoelectrochemistry, solar chemistry, photochemistry of semiconductor and metal nanoparticles, physical-chemical mechanisms of free radical reactions, and chemical engineering of photocatalytic processes. He has published more than 190 papers in peer-reviewed international journals. His publications have been cited more than 13 000 times (h-Index: 45).

1. Introduction

Mesoporous materials have attracted considerable interest for their applications as catalysts, gas separators, sensors, and energy converters.[1–4] The photocatalytic oxidation of organic pollutants in water and air as an advanced oxidation process has been proved to be an effective technique for environmental remediation. To develop efficient photocatalytic systems, high-quality semiconductor-based materials have been actively studied in recent years. Among a wide spectrum of semiconductors, TiO_2 has attracted significant attention over the past decades due to its excellent performance as a photocatalyst under UV light irradiation. Mesoporous TiO_2 is an interesting material for photocatalytic applications due to its continuous particle framework, which may be beneficial compared to separated individual nanoparticles, in particular for catalyst recovery. The reasons for the low number of studies made on ordered mesoporous TiO_2 as a photocatalyst are likely related to the difficulties in making it as an ordered material. Ever since Antonelli and Ying,[5] first synthesized mesoporous TiO_2 in 1995, many efforts have been made to control the crystallization and to make more crystalline material with maintenance of mesoscale order. Usually, mesoporous TiO_2 is prepared by template-based methods using soft templates (surfactants and block polymers) and hard templates (porous silica, polystyrene spheres, porous carbon).[6–9] However, the wall of these materials is normally amorphous, and under heat treatment, crystallization results in the collapse of the uniform mesoporous structure. Another approach to TiO_2-containing mesoporous materials for photocatalysis has been to modify the existing mesoporous SiO_2 with TiO_2. This has given good results and hence made it even more interesting to prepare ordered mesoporous (highly) crystalline TiO_2.[10,11] TiO_2 has been widely used as a photocatalyst for the removal of hazardous organic substances and as an electrode material for dye-sensitized solar cells[12,13] due to its strong oxidizing and reducing ability under UV light irradiation. Two of the most important factors affecting the photocatalytic activity of TiO_2 are its specific surface area in a continuous structure rather than in discrete particles and its crystallinity. This continuity can be expected to make the electron transfer within the material easier, resulting in higher activity. If mesoporous TiO_2 could be prepared with an anatase crystalline wall, it would be a useful material applicable as a high performance photocatalyst. In the last decade, research efforts have been directed to enhance the activity of the mesoporous TiO_2 photocatalysts using various methods such as increasing catalyst surface-to-volume ratio, sensitization of the catalyst using dye molecules,[14,15] doping the catalyst with nonmetals such as nitrogen, carbon, fluoride and iodine[16–19] and transition metals.[20–23] It has been demonstrated that the addition of a low percentage of noble metals such as Au, Pt, Ag, and Pd[24–26] to TiO_2 improves its photocatalytic activity. In the present review, the recent developments in the syntheses of mesoporous TiO_2 as active photocatalysts by the surfactant assembly will be presented. Also, this review focuses on the preparation and characterisation of mesoporous TiO_2, transitions metals ions, noble metals and nonmetal doped mesoporous TiO_2 networks as photoactive photocatalysts. The photocatalytic activity of mesoporous TiO_2 materials upon visible and UV illumination will be reviewed, summarized and discussed, in particular, concerning the influence of preparation and solid-state properties of the materials. Reaction mechanisms that are being discussed to explain these effects will be presented and critically evaluated.

2. Synthetic methods for mesoporous titania photocatalyst

Mesoporous TiO_2 as active photocatalysts could be prepared by different methods such as sol–gel, hydrothermal, sonochemical, microwave and electrodeposition (Table 1). In the past decade, mesoporous TiO_2 have been well synthesized with or without the use of organic surfactant templates. Templates were used as structure-directing agents for organizing network forming TiO_2 and mixed oxide species in nonaqueous solutions. The most commonly used organic templates were amphiphilic poly(alkylene oxide) block copolymers, such as $HO–(CH_2CH_2O)_{20}(CH_2CH(CH_3)O)_{70}$ $(CH_2CH_2O)_{20}$ H (designated $EO_{20}PO_{70}EO_{20}$, called Pluronic P-123)[24–27,33,37,38,53,70,71,86,89,92,107,119,130] and $HO(CH_2CH_2O)_{106}–(CH_2CH(CH_3)O)_{70}(CH_2CH_2O)_{106}H$ (designated $EO_{106}PO_{70}EO_{106}$, called Pluronic F-127).[73,80,81,100,102,106,113–117,131,135] Besides triblock copolymers as structure-directing agents, diblock polymers were also used such as $[C_nH_{2n-1}(OCH_2CH_2)_yOH$, Brij 56 (B56, *n*/*y*) 16/10][49] Other surfactants employed to direct the formation of mesoporous TiO_2 include tetradecyl phosphate by Antonelli and Ying[5] and commercially available dodecyl phosphate by Stone and Davis,[85] Tween 80, [57] tetradecylamine,[52] dodecylammonium chloride (DDAC)[17] and cetyltrimethylammonium bromide (CTAB) (Table 1).[29–32,43,45–47,87,100]

TiO_2 is an interesting material for photocatalytic applications and it is regarded as the most efficient and environmentally benign photocatalyst, and it has been most widely used for photodegradation of various pollutants such as methylene blue (MB),[30,37,52,55,57] methyl orange (MO),[30,39] *Escherichia coli* (*E. coli*),[57,60] Rhodamine B (RhB)[36,46–48] Rhodamine 6G (Rh6G)[29] and phenol[27,47] (Table 1).The principle of the semiconductor photocatalytic reaction is straightforward. When photons with energies >3.2 eV, *i.e.*, exceeding the band gap energy of TiO_2, are absorbed by the anatase particles in the mesoporous TiO_2 photocatalysts electrons are rapidly promoted from the valence band to the conduction band leaving holes behind in the valence band.[61] The thus formed electrons and holes participate in redox processes at the semiconductor/water interface. The valance band holes migrate to the surface of the particles where they react with adsorbed hydroxide ions (or water molecules), generating adsorbed ·OH radicals. This photodecomposition process usually involves one or more radicals or intermediate species such as ·OH, $O^{\cdot-}$, H_2O_2, or $O_2^{\cdot-}$, which play important roles in the photocatalytic reaction mechanisms.[61] The photocatalytic activity of a semiconductor is largely controlled by (i) the light absorption properties, *e.g.*, light absorption spectrum and coefficient, (ii) reduction and oxidation rates on the surface by the electron and hole, and (iii) the electron–hole recombination rate.[61]

2.1. Sol–gel method

Using the sol–gel process, a colloidal suspension, or a sol, is formed from the hydrolysis and polymerization reactions of the

Table 1 Synthesis routes and textural properties of mesoporous TiO_2 nanoparticles and their photocatalytic degradation of organic pollutants from both aqueous and air streams[a]

Synthesis routes	Template	$P_{S\ TiO2}$/nm	TiO_2 phase	S_{BET}/m^2g^{-1}	$Vp/cm^3\ g^{-1}$	Dp/nm	Pollutants	Ref.
Sol–gel	CTAB		A	340	0.28	3.2	Rh6G	29
		5	A	281	0.263	5	MB, BP, MO	30
			A	262		4	2-Propanol	45
	Tween	9.2	A	147	0.221	4	MB, *E. coli*	57
	P104	5–7	A			7–9	Stearic acid	59
	P123	13.2	A + R	91.7	0.187	4.5	Phenol	27
		5.5	A	175			CH_3Br	58
		2.3	A + R	171		4.6	Benzene	33
			A + R	200		6.7	HCHO and MB	37
	Polymer brush	12 ± 2	A	34			RhB	36
	SiO_2 microspheres	2.2 μm	A	174		10–110	MO	39
	PEO and PEG	10	A	214			*E. coli*	60
Hydrothermal	CTAB	6–11	A + B	140	0.4	2.2	RhB and phenol	47
		2.3	A	317	0.61	2.5	RhB	48
	None	300	A	168		12	RhB	50
		8.8	A + B	156	0.35	7.6	Acetone	44
	TEA	10	B + R	71		20	RhB	46
Electrochemical	TMAH	10	A			8	MB	55
	None	15	A + R	140			CH_3CHO	56
Microwave	TDA	100	A	90.4	0.15	5	MB	52
Sonochemical	P123	7.7	A + B	112	0.24	6.7	*n*-Pentane	53 and 54

[a] Methyl orange (MO), bromopyrogallol red (BP), methylene blue (MB), *Escherichia coli* (*E. coli*), Rhodamine B (RhB), Rhodamine 6G (Rh6G), tetramethylammoniumhydroxide (TMAH), poly-(ethylene oxide)–poly(propylene oxide)–poly(ethyleneoxide) (EOx–POyEOx), $EO_{18}PO_{58}EO_{18}$ (P104), polyethylene oxide (PEO) and polyethylene glycol (PEG), triethylamine (TEA), Tetradecylamine (TDA), anatase (A), rutile (R), brookite (B), S_{BET} surface area, $P_{S\ TiO2}$ average particle size of TiO_2 nanoparticle, Vp pore volume and Dp pore diameter.

precursors, which are usually inorganic metal salts or metal–organic compounds. Complete polymerization and loss of solvent leads to the transition from the liquid sol into a solid gel phase. First, a homogeneous solution is obtained by dissolving the surfactant(s) in a solvent. TiO_2 precursors are then added into the solution where they undergo hydrolysis catalyzed by an acid catalyst and transform to a sol of Ti–O–Ti chains.[27–34,37] Chen *et al.*,[27] prepared mesoporous TiO_2 using $TiCl_4$ and Ti $(OBu)_4$ as the precursors and P123 as the template by the nonhydrolytic evaporation-induced self-assembly (EISA) method with ordered 3-D TiO_2 (Fig. 1). Photodegradation of phenol shows that the mesoporous TiO_2 has a better photoactivity than the commercial TiO_2 P25. This is attributed to the well ordered 3D open-pore structure, which, combined with its relatively large surface area and pore volume, can facilitate the mass transport of the organic pollutants. Therefore, both the regular open pore morphology and the biphasial structure are playing crucial roles in determining the sample's photoactivity.

Beyers *et al.*, have reported the preparation of mesoporous TiO_2 using CTAB as surfactant.[29] The photocatalytic activity of mesoporous TiO_2 for the decomposition of Rhodamine 6G could be increased by changing the synthesis medium from basic to acidic conditions. The use of different surfactants under the same conditions results in a different moment on which the anatase is formed during the synthesis procedure. A possible explanation has to be found in the differences in interactions between the TiO_2 and the surfactant.[29] The slower condensation of the TiO_2 precursor leads to a better formed mesoporous structure, with better accessibility for photocatalysis. Moreover, TiO_2 anatase has been prepared by using the sol–emulsion–gel method in the presence of both CTAB[30–32] and cyclohexane. The as-prepared anatase powders exhibited high photocatalytic activity and could be effectively used as catalyst for photodegradation of methyl orange, bromopyrogallol red, and methylene blue. Shiraishi *et al.*,[33] have developed highly selective methods for photochemical organic synthesis, driven by a mesoporous TiO_2,[34] which enables a transformation of benzene into phenol,

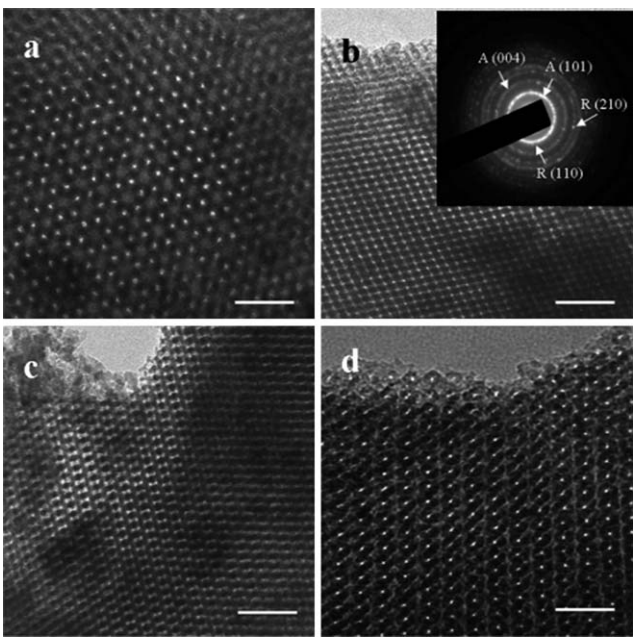

Fig. 1 TEM images of the typically prepared sample viewed from the following planes: (a) [111]; (b) [110]; (c) [311]; (d) [100]. Scale bar: 50 nm. Inset: ED patterns. Reprinted with permission from ref. 27, Copyright 2007 ACS.

with very high selectivity (>80%). The system proposed exhibits significant advantages for organic synthesis: (i) additive-free, (ii) cheap source of oxidant, and (iii) mild reaction condition. Liu *et al.*,[35] have prepared nanostructured anatase TiO_2 monoliths using 1-butyl-3-methylimidazolium tetrafluoroborate ($BMIM^+BF^-_4$) ionic liquids as template solvents by a simple sol–gel method with a peptization process at ambient temperature. The as-prepared products showed wormhole-like mesoporous structures and mesoporous structures of the product with a surface area of *ca.* 260 $m^2\ g^{-1}$ were retained upon calcining to 450 °C, showing excellent thermal stability. Furthermore, the products revealed higher photodegradation ability towards Rhodamine B than that of the commercially available TiO_2 P25. Lu *et al.*,[36] have synthesized well-defined, crystalline TiO_2 nanoparticles at room temperature by using spherical polyelectrolyte brush particles as a template. The template particles consist of a polystyrene core from which long chains of poly(styrene sodium sulfonate) are grafted. $Ti(OC_2H_5)_4$ is hydrolyzed in the presence of brush particles leading to the formation of well-dispersed TiO_2 nanoparticles. The as-prepared TiO_2 nanocomposites present high photocatalytic activity for the degradation of Rhodamine B under UV irradiation.

Long TiO_2 hollow fibers with mesoporous walls employing the sol–gel method combined two-capillary spinneret electrospinning technique using a P123 have been fabricated.[37,38] The photodegradation rate of methylene blue (MB) and gaseous formaldehyde for the TiO_2 hollow fibers was faster than that for P25 and mesoporous TiO_2 powders. Yu *et al.*,[39] have prepared TiO_2 hollow microspheres, based on template-directed deposition and *in situ* template-sacrificial dissolution, which was developed in pure water by using SiO_2 microspheres as templates and TiF_4 as the precursor at 60 °C (Fig. 2). It is found that the prepared TiO_2 hollow microspheres show a stronger absorption in the UV-visible region (310–700 nm) than the nanoporous structures of P25. Thus, this also leads to an enhanced photocatalytic activity of the TiO_2 hollow spheres. Shibata *et al.*,[40] have succeeded in synthesizing crystallized mesoporous titania using sol–gel reaction of $TiOSO_4$ in the presence of CTAB at various temperatures. The combination of a $TiOSO_4$ precursor and a CTAB template with quaternary ammonium ions affects the formation rate of anatase crystal nuclei at the surface of the assemblies. Optimization of the composition of these two components and the temperature leads to the formation of anatase crystalline particles while maintaining the hexagonal pore structure. Under UV light irradiation, the concentration of 2-propanol decreased and acetone was generated. The results suggest that the obtained mesoporous material thus prepared has good adsorbability as well as photocatalytic activity.

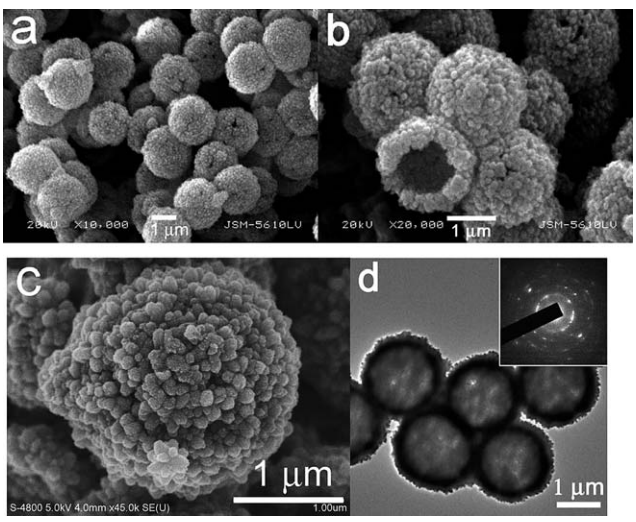

Fig. 2 (a and b) SEM, (c) FESEM, and (d) TEM images of TiO_2 hollow spheres obtained in a 0.02 M TiF_4 aqueous solution at 60 °C for 12 h. Inset in (d) shows the SAED pattern of individual TiO_2 hollow sphere. Reprinted with permission from ref. 39, Copyright 2008 ACS.

2.2. Hydrothermal method

Hydrothermal synthesis is normally conducted in steel pressure vessels called autoclaves with Teflon liners under controlled temperature and/or pressure with the reaction occurring in aqueous solutions. The temperature can be elevated above the boiling point of water, reaching the pressure of vapor saturation. The temperature and the amount of solution added to the autoclave largely determine the internal pressure produced. Many groups have used the hydrothermal method to prepare mesoporous TiO_2 nanoparticles.[41–51]

Formation mechanism of stable porous TiO_2. TiO_2 crystallites with low crystallinity are first prepared by a hydrolysis process in the acid system, and it can be expected that they easily form agglomerations because of the existence of some amorphous phase resulting from Ti(OH)*n*.[41] Subsequently, the CTAB introduction during the hydrothermal process under basic conditions can effectively disperse the agglomeration and further induce the assembly of the as-prepared crystallites. Under basic conditions, the CTA^+ groups are always positively charged, while the nanoparticles are negatively charged (Fig. 3). Thus, the strong interaction between the nanoparticles and CTAB, resulting from the electrostatic attraction, results in the dispersion of nanoparticles together with the transformation from amorphous to TiO_2 crystallites and further induces the assembly of the as-prepared crystallites to form mesoporous TiO_2.[41–43,47,48]

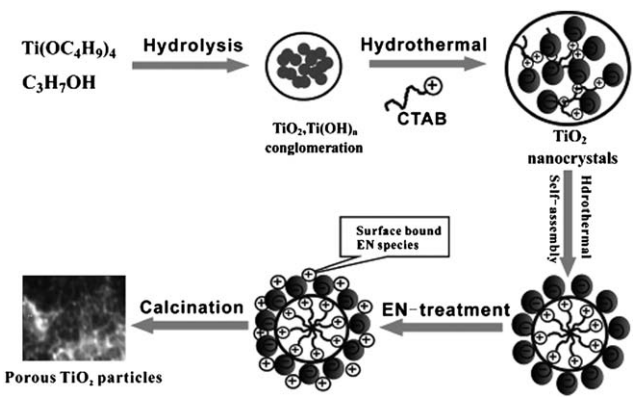

Fig. 3 Scheme of idealized formation model of stable porous TiO_2 nanoparticles. Reprinted with permission from ref. 47, Copyright 2008 ACS.

Mesoporous TiO_2 with an amorphous wall can be prepared using $Ti(SO_4)_2$ in the presence of the cationic surfactant CTAB at room temperature.[43] The large surface area, small crystalline size, and well-crystallized anatase mesostructure can explain the high photocatalytic activity of mesoporous TiO_2 nanoparticles calcined at 400 °C for the photodegradation of Rhodamine B.[48] Mixed-phase TiO2 nanocrystals with tunable brookite-to-rutile ratios using TiCl4 and triethylamine[46] and using CTAB as the template have been synthesized, followed by a post treatment in the presence of ethylenediamine.[47] Interestingly, the prepared TiO_2 photocatalysts showed higher photocatalytic efficiency than Degussa P25 in the degradation of phenol and Rhodamine B in aqueous solution under UV irradiation.

Trimodally sponge-like macro-/mesoporous titania was prepared by hydrothermal treatment of precipitates of $(Ti(OC_4H_9)_4)$ in pure water.[45] The prepared TiO_2 samples exhibit a disordered worm-like macroporous frameworks with continuous nanocrystalline titania particles (Fig. 4). The hierarchically porous titania prepared at 180 °C for 24 h displayed an especially high photocatalytic activity for acetone decomposition probably due to its special pore-wall structure, and its photocatalytic activity was about three times higher than that of Degussa P25.

Wang *et al.*,[49] have synthesized mesoporous TiO_2 using TTIP and nonionic poly(alkylene oxide)-based surfactant (decaoxyethylene cetyl ether,$C_{16}(EO)_{10}$, Brij 56) as the structural-directing agent. The catalyst which was calcined at 350 °C possessed an intact macro/mesoporous structure and showed photocatalytic reactivity for ethylene oxidation 60% higher than that of P25. Further heating at temperatures above 600 °C destroyed both macro- and mesoporous structures, accompanied by a loss in photocatalytic activity.[49] The high photocatalytic performance of the intact macro/mesoporous TiO_2 may be explained by the existence of macrochannels that increase photoabsorption efficiency and allow efficient diffusion of gaseous molecules. Liu *et al.*,[50] have synthesized porous TiO_2 hollow aggregates on a large scale by a hydrothermal method without using any templates. The photocatalyticRhodamine B degradation rate of the porous TiO_2 hollow aggregates is found to be more than twice that of P25. The higher photocatalytic activity of the porous TiO_2 hollow aggregates can be explained by considering several factors: The larger specific surface area (porous TiO_2 hollow aggregates *ca.* 168 $m^2 g^{-1}$ *versus* Degussa P25 powder *ca.* 45 $m^2 g^{-1}$); hence, there are more reactant adsorption/desorption sites for catalytic reactions. (2) The prevention of the unwanted aggregation of the nanoparticle clusters, which is also helpful in maintaining the high active surface area. (3) The highly porous structure, which allows rapid diffusion of various reactants and products during the reaction. (4) The smaller crystal size, which means more powerful redox ability owing to the quantum-size effect; moreover, the smaller crystal sizes are also beneficial for the separation of the photogenerated hole and electron pairs.[50,51]

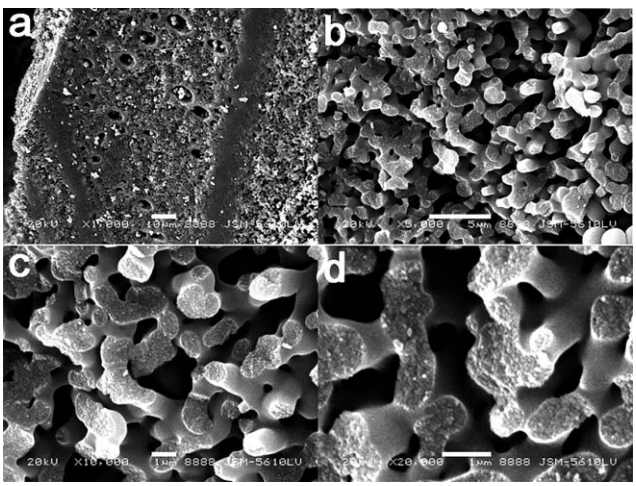

Fig. 4 SEM images of hierarchically sponge-like macro-/mesoporous titania prepared at 180 °C for 0 (a), 1 (b), 10 (c), and 24 h (d). Reprinted with permission from ref. 45, Copyright 2007 ACS.

2.3. Microwave method

A dielectric material can be processed with energy in the form of high-frequency electromagnetic waves. The principal frequencies of microwave heating are between 900 and 2450 MHz. Microwave radiation has been applied to prepare various mesoporous TiO_2 nanoparticles in the presence of tetradecylamine surfactant. Crystalline mesoporous anatase with wormhole-like pore sizes of 3–5 nm and particle sizes 100–300 nm were prepared by a modified sol–gel process of TTIP, accelerated by a microwave hydrothermal process.[52] Mesoporous wormhole-like and crystalline powders with surface areas of 243–622 $m^2 g^{-1}$ are obtained. It is shown that crystallization by calcination at 400 °C per 3 h inevitably reduced the surface area, while the microwave hydrothermal process demonstrated a rapid formation of crystalline mesoporous TiO_2 nanopowders with a high-surface area and excellent photocatalytic effects for MB photodegradation.[52]

2.4. Sonochemical method

Ultrasound has been very useful in the synthesis of mesoporous TiO_2 active photocatalysts.[53,54] Yu *et al.*[53,54] applied the sonochemical method in preparing highly photoactive TiO_2 nanoparticles with anatase and brookite phases using the hydrolysis of TTIP in pure water or in a 1 : 1 EtOH–H_2O solution under ultrasonic radiation in the presence of P123[53] or without template.[54] Both as-prepared samples exhibited better activities than the commercial TiO_2 P25 in the degradation of *n*-pentane in air (Fig. 5). The degradation rate of mesoporous TiO_2 was about two times greater than that of P25. The high activities of the mesoporous TiO_2 with a bicrystalline framework can be attributed to the combined effect of three factors: high brookite content, high surface area, and the existence of mesopores.

2.5. Electrodeposition

Electrodeposition is commonly employed to produce a coating, usually metallic, on a surface by the action of reduction at the cathode. TiO_2/benzoquinone hybrid films have been electrodeposited anodically from basic Ti(IV)-alkoxide solutions containing hydroquinone in the presence of tetramethylammoniumhydroxide.[55] The photodegradation of MB as a representative for organic pollutants has been studied. The results revealed that the amorphous film calcined at 350 °C is quite inactive but the activity increases with increasing calcination temperature with the exception of the film calcined at 500 °C. Matsumoto

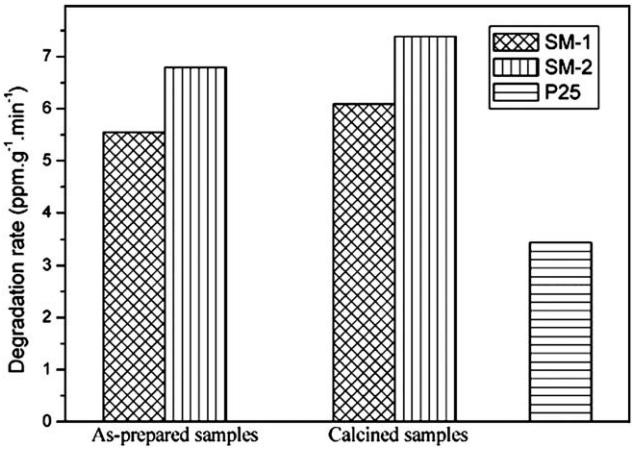

Fig. 5 Photocatalytic activities of the as-prepared and calcined SM-1 without P123, SM-2 with P123, and P25 for degradation of *n*-pentane in air. Reprinted with permission from ref. 53, Copyright 2002 ACS.

et al., have prepared a mesoporous TiO_2 photocatalyst film onto alumite using an electrochemical technique,[56] where the initial electrodeposition was carried out by electrolysis in $(NH_4)_2[TiO(C_2O_4)_2]$ solution, followed by pulse electrolysis in $TiCl_3$. This film had a high catalytic activity for the decomposition of acetaldehyde, with CO_2 at with the corresponding concentration being detected in the cell after 45 min even under fluorescent lamp illumination.

2.6. Mesoporous TiO_2 thin films as active photocatalysts

Various TiO_2 sols containing poly(oxyethylenesorbitan monooleate) (Tween 80) surfactant to tailor-design the porous structure of TiO_2 using dip-coating at different molar ratios of Tween 80/isopropyl alcohol/acetic acid/TTIP $= R: 45: 6: 1$ have been synthesized.[57] The prepared TiO_2 photocatalytic membrane has great potential in developing highly efficient water treatment and reuse systems, for example, decomposition of organic pollutants, inactivation of pathogenic microorganisms, physical separation of contaminants, and self-antifouling action because of its multifunctional capability. Wang *et al.*,[58] have obtained 3D ordered mesoporous sulfated-TiO_2 reacting a cubic mesoporous amorphous TiO_2 film with sulfuric acid at high temperature to produce sulfur-containing mesoporous TiO_2 with nanocrystalline frameworks. The resulting 3D ordered mesoporous sulfated-TiO_2 superacids are found to be attractive photocatalysts for degradation of bromomethane. High-quality mesostructured titania thin films have been prepared on silicon substrates by spin coating(Fig. 6).[59] Their thermal stability can be greatly enhanced from about 350 to 850 °C using a supercritical fluid post-treatment process. High-temperature calcination of the films leads to formation of nanocrystals of anatase within the pore walls without causing collapse of the mesoporous structure (Fig. 6). A 0.02 M solution of stearic acid in methanol was first coated on the titania-coated silicon wafers by spin coating. The decrease in the stearic acid concentration with the sc-CO_2/TTIP-treated film is considerably faster compared to the untreated and sc-CO_2/TMOS treated films. The higher efficiency can be explained by its high porosity and the presence of its highly

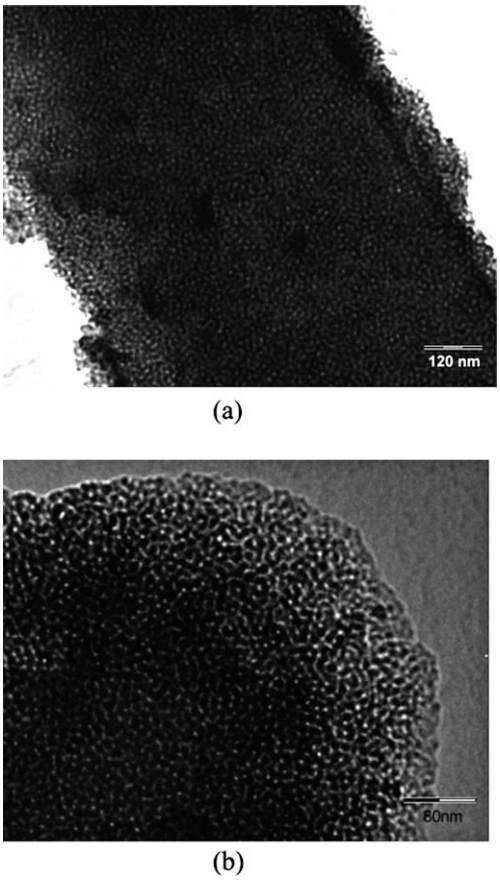

Fig. 6 TEM images of mesoporous titania thin films calcined at (a) 750 and (b) 850 °C, respectively, after sc-CO_2/TTIP treatment. Reprinted with permission from ref. 59, Copyright 2005 ACS.

photoactive anatase nanocrystalline structure. Without sc-CO_2 treatment calcination at temperatures above 550 °C inevitably leads to collapse of the ordered mesoporous structure and formation of rutile crystallites in the walls of the TiO_2 thin films from the transformation of anatase nanocrystals.[59]

Kim and Kwak,[60] have prepared monodisperse spherical mesoporous TiO_2 with a morphology size of ~800 nm *via* the sol–gel approach using a triblock copolymer surfactant and titanium TTIP with 2,4-pentanedione in aqueous solution. It was coated onto glass substrates without cracking by using the doctor blade method with various amounts of polyethylene oxide (PEO) and polyethylene glycol (PEG) (Fig. 7). The results revealed that the efficiency of photocatalytic disinfection with the film adhesion method is strongly dependent on the surface area and crystallite size.

In general, the direct synthesis of mesoporous materials with a crystalline wall has been considered to be difficult for several reasons. One major reason is that phase transformation from amorphous to crystalline by heat treatment or UV light irradiation usually induces the collapse of mesopores because the wall is too thin to retain the 3-D mesoporous structure during crystallization. Direct synthesis of crystalline mesoporous TiO_2 without any supports requires deposition of very fine TiO_2 crystalline particles on the nanoscale surface of surfactant molecular assemblies. Mesoporous TiO_2[27–40] prepared by sol–gel

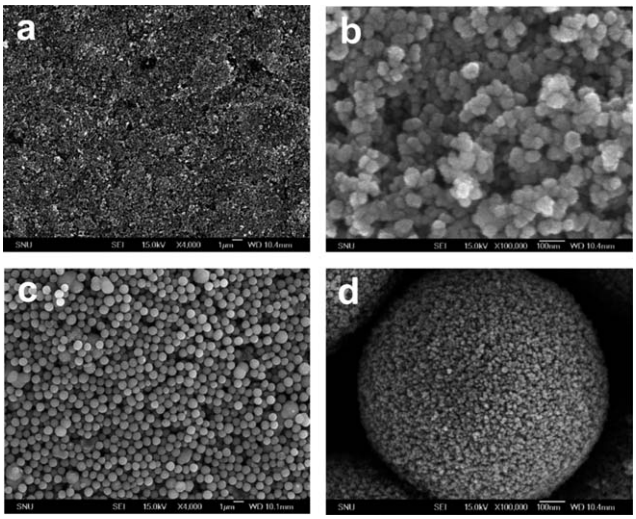

Fig. 7 SEM images of TiO_2 coated with 40 wt% of PEG and PEO and calcined at 400 °C. (a) A P25 TiO_2 coated sample, (b) a magnified image of the P25 TiO_2 coated sample, (c) a monodisperse spherical mesoporous TiO_2 coated on glass, (d) a magnified image of the coated mesoporous TiO_2. Reprinted with permission from ref. 60, Copyright 2009 ACS.

reaction using surfactant lyotropic liquid crystals as the reaction template has gathered considerably as one of the best techniques. However, the wall of these materials is normally amorphous, and under heat treatment, crystallization results in collapse of the uniform mesoporous structure. Shibata *et al.*, have succeeded to synthesize highly ordered mesoporous TiO_2 with crystalline walls by the sol–gel method.[40] Also, hydrothermal treatment is considered one of the most efficient methods to prepare disordered mesostructure TiO_2.

The reason of high photocatalytic activity of mesoporous TiO_2 is explained by: (i) the larger specific surface area of mesoporous TiO_2 *versus* Degussa P25 powder; hence, there are more reactant adsorption/desorption sites for catalytic reactions. (ii) The prevention of the unwanted aggregation of the nanoparticle clusters, which is also helpful in maintaining the high active surface area. (iii) The highly porous structure, which allows rapid diffusion of various reactants and products during the reaction. (iv) The smaller crystal size, which means more powerful redox ability owing to the quantum-size effect; moreover, the smaller crystal sizes are also beneficial for the separation of the photogenerated hole and electron pairs.

3. Transition metal doped mesoporous TiO_2

Anatase TiO_2 can only be excited by UV irradiation ($\lambda < 380$ nm) because of its large band gap energy of 3.2 eV. Moreover, the rapid recombination of photoinduced electrons and holes greatly lowers the quantum efficiency.[61] Therefore, it is of great interest to improve the generation and separation of photoinduced electron–hole pairs in TiO_2 for further applications. The manipulation of semiconductor heterostructures has been shown to be one of the effective methods for photoinduced electron–hole generation and separation in recent years.[62,63] Multiple-semiconductor devices can absorb a larger fraction of the solar spectrum, which is beneficial for the excitation of the semiconductor and thus the photoinduced generation of electrons and holes. Moreover, the coupling of two different semiconductors could transfer electrons from an excited small band gap semiconductor into another attached one in the case of proper position of the conduction band potentials (Table 2). This favors the separation of photoinduced electrons and holes and thus improves the photocatalytic efficiency of the semiconductor heterostructure dramatically.

3.1. Fe (III) doped TiO_2

Xuan *et al.*,[64] have prepared well-defined magnetically separable, hollow spherical Fe_3O_4/TiO_2 hybrid photocatalysts through a poly(styrene-acrylic acid) (PSA) template method (Fig. 8). These Fe_3O_4/TiO_2 hybrid hollow spherical with hollow nature exhibit good photocatalytic activity for the degradation of RhB under UV light irradiation and can be recycled six times by magnetic separation without major loss of activity.

Kim *et al.*,[65] have synthesized mesoporous iron oxide-layered titanate nanohybrids through a reassembling reaction between exfoliated titanate nanosheets and iron hydroxide nanoclusters, in which an electrostatic attraction between both nanosized species could be achieved at a low pH of 1.5. The photocatalytic activity revealed that the present nanohybrids could induce the photodegradation of methylene blue and DCA under visible light illumination ($\lambda > 420$ nm). Fe-doped nanocrystalline TiO_2 with a mesoporous structure was prepared *via* a facile nonhydrolytic sol–gel route.[66,67] During photodegradation of MB under visible light irradiation, as-prepared Fe/TiO_2 exhibited a higher activity than either the undoped TiO_2 or the Fe/TiO_2 obtained *via* the traditional hydrolytic sol–gel route. The promoting effect of the Fe-doping on the photocatalytic activity for MB decomposition could be attributed to the formation of intermediate energy levels that allow Fe/TiO_2 to be activated easily in the visible region. The nonhydrolytic sol–gel method is superior to the traditional hydrolytic sol–gel method owing to the controllable reaction rate and lack of surface tension, which ensures the formation of mesopores and well-crystallized anatase in the Fe/TiO_2 sample, leading to a higher activity since the reactant molecules are easily adsorbed and the recombination between the photoelectrons and the holes is effectively inhibited.[66] A new multifunctional nanocomposite (Fe*x*O*y*@Ti–hexagonal mesoporous silica (HMS)) involving superparamagnetic iron oxide nanoparticles, and ordered mesoporous channels has been developed *via* the coating of as-synthesized iron oxide nanoparticles with an amorphous silica layer followed by the sol–gel polymerization using TEOS, tetrapropyl orthotitanate (TPOT), and a structure-directing reagent.[68] The Fe*x*O*y*@Ti–HMS acted as an efficient heterogeneous catalyst for the liquid-phase selective oxidation reactions of organic compounds using hydrogen peroxide (H_2O_2) as an oxidant. The bifunctional composites were synthesized by wet impregnation, drying, ethanol washing, and a calcination process.[69] The meso-TiO_2/α-Fe_2O_3 composites possess synergy of the photocatalytic ability of meso-TiO_2 for oxidation of As(III) to As(V) and the adsorption performance of α-Fe_2O_3 for As(V). The results show that the *meso*-TiO_2/α-Fe_2O_3 composites can oxidize higher toxic As(III) to lower toxic As(V) with high efficiency at various pH values by a photocatalytic reaction. At the same time, As(V) is effectively removed by adsorption onto the surface of

Table 2 Synthesis routes and textural properties of doped oxides into mesoporous TiO_2 and their photocatalytic degradation of organic pollutants from both aqueous and air streams[a]

Synthesis routes	Oxides	Template	$P_{S\ TiO2}$/nm	TiO_2 phase	S_{BET}/m^2g^{-1}	Vp/$cm^3\ g^{-1}$	Dp/nm	Pollutants	Ref.
Sol–gel	Fe_3O_4/or Fe_2O_3	Latex	10	A				RhB	64
		None			230		6–12	MB and DCA	65
		None	10	A	156	0.31	3	MB	66
		HMS			910		3	2,6-DTBP	68
		None		A	95			As(III)	69
Sol–gel	SiO_2	P123	10	A	290	0.27	6.8	RhB	92
		P123		A	198	0.21	6.93	Phenol	93
		SBA-15		A	848	1.08	8.7	Orange II	94
		CTAB	9.2	A	645	0.53	2	Benzene	95
		PMAA	206	A				MO	97
		MCM-41	10–25	A	725	0.6	3.3	R-6G	99
		PAH		A				Orange II	102
		CTAB			915			NO	105
		P123	5		52	0.21	6–7	NO	108
		P123 or F127	5–14	A	167	0.23	9–11	NO	109
Hydrothermal		None	8.9	A	238	0.58	9.8	Phenol	96
		F127	10	A	118		2–3	RhB	103
Sol–gel	Bi_2O_3	P123	4–12	A	50–167	0.29	6–7	CP	70 and 71
	BiOI	None	3		39.3	116		MO	72
Sol–gel	Cr_2O_3	F127	11.5	A	135		3.2	MB	73
		MCM-48			1437	0.9	1.8	CH_3CHO	78
Sol–gel	RuO_2	None	39	A	51	0.08	28	Acetone	79
		F127	9.7	A	165	0.25	7.7	Methanol	80
Sol–gel	ZrO_2	Tween 60		A	43			SA and 2-CP	21
Hydrothermal	F^- and ZrO_2	None		A	97	0.3	12	Toluene	82
Sol–gel	CeO_2	HDA		A				Toluene	20
		CTAB	9	A	847	0.54	2.7	Acetone	83
Hydrothermal	Niobia	DDP		A	415			Propanol	85
Sol–gel	H_3PO_4	P123	6.5	A	222	0.5	5.2	*n*-Pentane	86
Sol–gel	La_2O_3	None		A				Phoxim	87
Hydrothermal		CTAB	4.5	A	243	0.56	3	RhB	88
Solvothermal	Ag/In_2O_3	P123	22	A + R	74	0.27	16.5	RhB and MTBE	89
Sol–gel	Ag, Co, Cu, Fe, and Ni	None	44	A + R	30		13.2	AP and NB	22
	NiO	None	8	A	169		5.5	Methanol	23
Sol–gel	WO_3	F127	10	A				Propanol	81

[a] Methyl orange (MO), methylene blue (MB), Rhodamine B (RhB), Rhodamine 6G, PMAA poly(methacrylic acid) (PMAA), Rhodamine B (RB), methyl *tert*-butyl ether (MTBE), 2,6-di-*tert*-butyl phenol (2,6-DTBP), polyelectrolyte poly allylamine hydrochloride (PAH), octadecyltrimethylammonium chloride (ODAC), salicylic acid (SA), hexadecylamine(HDA). Dodecyl phosphate (DDP), acetophenone (AP) and nitrobenzene (NB), S_{BET} surface area, $P_{S\ TiO2}$ average particle size of TiO_2 nanoparticle, Vp pore volume and Dp pore diameter.

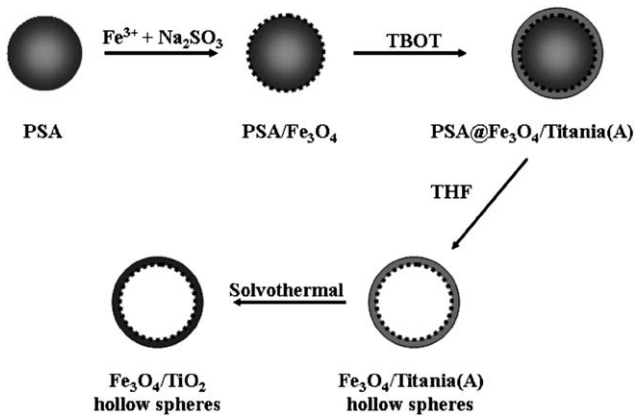

Fig. 8 Schematic procedure used for fabrication of magnetic TiO_2 hollow spheres (A: amorphous). Reprinted with permission from ref. 64, Copyright 2009 ACS.

composites. Tayade *et al.*,[22] have prepared mesoporous nanocrystalline TiO_2 by hydrolysis of TTIP, and the band gap of the TiO_2 was modified with transition metal ions Ag, Co, Cu, Fe, and Ni having different work functions by the wet impregnation method. The investigations were carried out to demonstrate the effect of ionic radius and work function of metal ions on photocatalytic activity of mesoporous TiO_2 for degradation of acetophenone (AP) and nitrobenzene (NB) in aqueous medium under ultraviolet light irradiation. The initial rate of the photocatalytic degradation of AP and NB varies due to the change in band gap of the catalyst, the work function, the ionic radii, and the position of the impregnated metal ions on the TiO_2 lattice. The silver impregnated catalysts showed the highest initial rate of photocatalytic degradation for both compounds due to the interstitial position of impregnated silver metal ion in the TiO_2 lattice.[22]

3.2. Bi(III) doped TiO_2

Bi_2O_3/TiO_2 nanocrystallines with ordered mesoporous structure have been synthesized by the EISA method using P123 surfactant as a template.[70] The Bi_2O_3-photosensitization of TiO_2 could extend the spectral response from UV to visible area, making the Bi_2O_3/TiO_2 photocatalyst easily activated by visible light for the

degradation of *p*-chlorophenol. The ordered mesoporous channels facilitate the diffusion of reactant molecules. Meanwhile, the high surface area could enhance the Bi_2O_3 dispersion, the light harvesting, and the reactant adsorption. Furthermore, the highly crystallized anatase may promote the transfer of photoelectrons from bulk to surface and thus inhibit their recombination with photoholes, leading to enhanced quantum efficiency. Besides the excellent activity, the recycling test also demonstrated that this catalyst was quite stable during liquid-phase photocatalysis since no significant decrease in activity was observed even after being used repetitively for 10 times, showing a good potential for practical applications. Kong *et al.*,[71] have prepared visible-light-driven mesoporous bismuth titanate photocatalyst, which possesses wormlike channels, mixed phase mesostructured frameworks, large pore diameter (~6.1 nm), and low band gap energy (2.5 eV) *via* a modified EISA. The calcined sample exhibited visible-light photocatalytic reactivity as shown by the degradation of 2,4-DCP in aqueous media. Zhang *et al.*,[72] have synthesized BiOI/TiO_2 heterostructures with different Bi to Ti molar ratios through a simple soft-chemical method at a temperature as low as 80 °C. The photocatalytic activities of these BiOI/TiO_2 were evaluated for the degradation of methyl orange under visible-light irradiation (λ > 420 nm). The results revealed that the BiOI/TiO_2 heterostructures exhibited much higher photocatalytic activities than pure BiOI and TiO_2, respectively, and 50% BiOI/TiO_2 showed the best activity among all prepared heterostructured photocatalysts at different BiOI/TiO_2 ratios. The visible-light photocatalytic activity enhancement of BiOI/TiO_2 heterostructures could be attributed to its strong absorption in the visible region and to the low recombination rate of the electron–hole pairs because of the heterojunction formed between BiOI and TiO_2.

3.3. Cr(III)and Ru(IV) doped TiO_2

Yu *et al.*[73] have fabricated an ordered and well-crystallized cubic Im3m mesoporous Cr–TiO_2 photocatalyst. Mesoporous TiO_2 is ineffective under visible light but the mesoporous Cr–TiO_2 shows a very high decomposition rate.[73,74] This must be due to the Cr^{3+} doping, which allows activation of the mesoporous TiO_2 sample in the visible light region. The excellent photocatalytic performance is also related to the open mesoporous architecture with a large surface area, good anatase crystallinity and a 3D-connected pore system. It is known that chemical reactions are most effective when the transport paths through which molecules move into or out of the nanostructured materials are included as an integral part of the architectural design.[75,76] The 3D-interconnected mesochannels in the cubic mesoporous Cr–TiO_2 composite serve as efficient transport paths for reactants and products in photocatalytic reactions.[77] However the Ti-Cr-MCM-48 photocatalyst prepared in a single step exhibits far superior photocatalytic activity compared to the TiO_2–Cr–MCM-48 prepared by a post-impregnation method. The catalysts were examined for the photocatalytic degradation of acetaldehyde under visible light. Ti-Cr-MCM-48 prepared in a single step showed the highest activity for CO_2 production. The high activity of Ti-Cr-MCM-48 arises from the synergistic interaction of the Cr ions dispersed in the MCM-48 framework and the titania nanocrystallites anchored onto the pore walls of MCM-48. The highly dispersed chromium ions can be excited by visible-light radiation to form a CT excited state, involving an electron transfer from O^{2-} to Cr^{6+}.[78]

Mesoporous RuO_2–TiO_2 was prepared by homogeneous hydrolysis of $RuCl_3$, $TiOSO_4$ and urea at 100 °C. The results confirmed that RuO_2–TiO_2 is photoactive under visible light and there was no enhancement under UV light for photodegradation of acetone in the gaseous phase.[79] Ismail *et al.*,[80] have prepared mesoporous RuO_2–TiO_2 nanocomposites at different RuO_2 (0–10 wt%) through a simple one-step sol–gel route. The measured photonic efficiency $\xi = 0.53\%$ at 0.5 wt% RuO_2–TiO_2 nanocomposite for CH_3OH oxidation is maximal and further increase of RuO_2 loading up to 10 wt% gradually decreases this value. The cause for the visible photocatalytic behaviour is the incorporation of small amounts of Ru^{4+} into the anatase lattice. On the other hand, under UV light, addition of RuO_2 suppressed photonic efficiencies of TiO_2.[79,80]

3.4. WO_3 and ZrO_2 doped TiO_2

Pan and Lee,[81] have prepared highly ordered cubic mesoporous WO_3/TiO_2 thin films by spin coating *via* an EISA process. With the incorporation of WO_3 into TiO_2, the ordering of the mesopore structure has been appreciably improved. The characterization results suggest that the majority of incorporated W species are located at the surface of the mesopore wall instead of doping into the TiO_2 lattice, the photocatalytic activity of WO_3/TiO_2 thin films in decomposing 2-propanol in the gas phase was optimized at 4 mol% of WO_3 concentration (Fig. 9). Its photocatalytic activity was 2.2 times that of a mesoporous TiO_2 film and 6.1 times that of a nonporous TiO_2 film derived from a typical sol–gel method.

Liu *et al.*,[82] have produced codoped Zr^{4+} and F^- ions within anatase hollow microspheres by a fluoride mediated self-transformation strategy. Urea was used to catalyze the hydrolysis of aqueous mixtures of Ti $(SO_4)_2$ and $ZrOCl_2$ in the presence of NH_4F under hydrothermal conditions. The concomitant participation of F^- promotes lattice substitution of Ti^{4+} ions by Zr^{4+} and facilitates the transformation of surface-segregated amorphous ZrO_x clusters into Zr–F species. The better photocatalytic activity of fluorinated samples may be at least partially attributed to the presence of well-crystallized anatase with retention of small grain size, high specific surface area and porosity, as well as hollow microarchitecture. Codoping is associated with electron transfer-mediated charge compensation between the Zr/F impurities, which reduces the number of both bulk and surface defects and provides a stabilizing effect on the local structure. Moreover, these synergetic interactions influence the textural characteristics and surface states of the TiO_2 host, such that the photocatalytic activity with regard to the decomposition of gaseous toluene is enhanced. Also the formation of porous TiO_2/ZrO_2 networks using mixed titania/zirconia precursor solutions was achieved by a polymer gel templating technique.[21] The mixed TiO_2/ZrO_2 network structures exhibit higher surface areas than a corresponding pure titania network, and in a certain range of metal oxide compositions. The photocatalytic efficiencies of the TiO_2 and TiO_2/ZrO_2 networks have been assessed by monitoring the

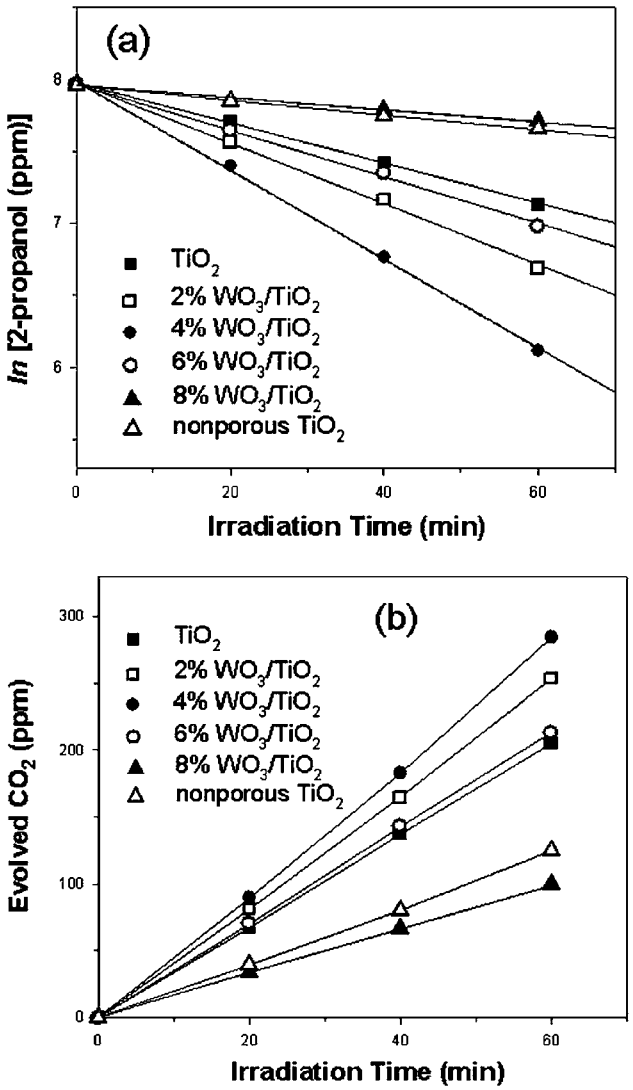

Fig. 9 Photocatalytic decomposition rate of 2-propanol to acetone (a) and evolution rate of CO_2 (b) with several cubic mesoporous and nonporous films. Reprinted with permission from ref. 81, Copyright 2006 ACS.

photodecomposition of two organic molecules: salicylic acid and 2-chlorophenol (2-CP). The TiO_2 network was found to exhibit an efficiency of ~60% and ~65% of the standard P25 TiO_2 for the salicylic acid and 2-CP reactions, respectively. For both photocatalytic reactions the presence of ZrO_2 in the TiO_2 network resulted in enhanced photocatalytic activity relative to the pure TiO_2 network, which is believed to be due to a number of factors including an increased surface area and a decrease of the anatase to rutile crystal phase transformation.

3.5. Ce (III) and Zn (II) doped TiO_2

Visible light induced metal-to-metal charge transfer (MMCT) for hetero-bimetallic Ti(IV)-O-Ce(III) assemblies on the pore of mesoporous silica, MCM-41 have been achieved.[83] The bimetallic Ti/Ce assembly exhibited the intense MMCT absorption up to 540 nm. The synthesis of Ti(IV)-O-Ce(III) assemblies on the pore of MCM-41 was made by applying the nucleophilic character of titanol groups of $(OH)Ti(OSi)_3$ sites. Namely, isolated $(OH)Ti(OSi)_3$ sites were first synthesized on the pore surface of MCM-41. Subsequently, dehydrated crystalline Ti-MCM-41 was added to a dry acetonitrile solution of Ce(III) NO_3 and stirred at 55 °C for 18 h. The pale yellow crystallites thus obtained were filtered, washed, and dried under dynamic vacuum at 40 °C. It was concluded that the catalytic oxidation of 2-propanol is driven by the visible-light induced MMCT of Ti (IV)-O-Ce(III) assemblies. Sinha and Suzuki,[20] have prepared a thermally stable mesoporous CeO_2–TiO_2 using hexadecylamine as structure-directing reagent and triethanolamine as an additive in mixed propanol–water medium. These novel mesoporous CeO_2–TiO_2 composites showed high performance for the photocatalytic removal of toluene. Kim *et al.*,[84] have investigated the chemical bonding character and physicochemical properties of mesoporous zinc oxide-layered titanate nanocomposites synthesized by an exfoliation–restacking route. Upon hybridization with ZnO nanoparticles, the photocatalytic activity of layered titanate is enhanced with respect to the oxidative photodegradation of phenol and dichloroacetate. But of greater importance is that the chemical stability of guest zinc oxide against acidic corrosion is greatly improved by hybridization with layered titanate.

3.6. Nb(v) and PO_4(III) and doped TiO_2

Stone and Davis[85] have prepared mesoporous titania and niobia molecular sieves by a ligand-assisted templating method. The transition metal oxides were tested as photocatalysts in the liquid-phase oxidative dehydrogenation of 2-propanol to acetone. The observed quantum yield of the reaction was 0.45 over P25. However, mesoporous titania converted 2-propanol with a very low quantum yield of 0.0026. A very low quantum yield was also found for the mesoporous niobia sample compared to a crystalline standard. The relative inactivity of mesoporous titania samples can be attributed to a high surface concentration of defects which can act as surface electron–hole recombination sites and/or the poisoning of catalytic surface sites by the phosphorus remaining from the surfactant. Yu *et al.*,[86] synthesized a phosphated mesoporous TiO_2 by incorporating phosphorus from phosphoric acid directly into the framework of TiO_2 *via* a surfactant-templated approach. It was found that the incorporation of phosphorus could stabilize the TiO_2 framework and increase the surface area significantly. This stabilization is attributed to two reasons: the more complete condensation of surface Ti–OH in the as-prepared sample and the inhibition of grain growth of the embedded anatase TiO_2 by the interspersed amorphous titanium phosphate matrix during thermal treatment. Both pure and phosphated mesoporous TiO_2 show significant activities for the oxidation of *n*-pentane. The higher photocatalytic activity of phosphated mesoporous TiO_2 can be explained by the extended band gap energy, large surface area, and the existence of Ti ions in a tetrahedral coordination.

Mechanism of phosphated mesoporous TiO_2. It is well-known that a large amount of uncondensed Ti–OH exists on the surface of the as-prepared amorphous mesoporous TiO_2. During calcination, the rapid reactions between the uncondensed Ti–OH

would cause the walls of mesoporous TiO_2 to collapse. This is why pure mesoporous TiO_2 has a relatively poor thermal stability. Reactions between phosphoric acid and uncondensed Ti–OH in the as-prepared phosphated mesoporous TiO_2 may result in more completely condensed walls, which effectively prevent the collapse of the mesoporous structure during calcination.[86]

3.7. Ni(II) and La(III) doped TiO_2

Jing *et al.*,[23] have prepared Ni–TiO_2 by using TBOT and acetylacetone in the presence of laurylamine. XRD and EDX results indicated that Ni^{2+} was incorporated into the framework of the mesoporous TiO_2 in a highly dispersed way. The results of photocatalytic hydrogen evolution from aqueous methanol solution under UV-vis light irradiation showed that the activity of hydrogen production strongly depended on the amount of Ni doped. The highest activity was achieved with Ni doping of 1%. The results were rationalized by assuming that Ni^{2+} serves as shallow trapping sites, greatly enhancing the activity of the mesoporous photocatalyst.

Dai *et al.*,[87] have prepared La-doped TiO_2 nanoparticles using $Ti(SO_4)_2$ and $La(NO_3)_3$ in the presence of CTAB. Photocatalytic degradation of commercial phoxim emulsion in aqueous suspension was investigated by using La-doped mesoporous TiO_2 as the photocatalyst under UV irradiation. La-doped TiO_2 with mesostructures showed much better photoactivity than undoped samples and P25, respectively due to its large surface area, highly crystallized mesoporous wall, and more active sites for concentrating the substrate.[88]

3.8. Multi-cations doped TiO_2

Yang *et al.*, have prepared silver and indium oxide codoped titania nanocomposites by a one-step sol–gel-solvothermal method in the presence of P123.[89] Silver nanoparticles have been photocatalytically deposited on mesoporous TiO_2 films.[90] The resulting Ag/In_2O_3–TiO_2 three-component systems mainly exhibited an anatase phase structure, high crystallinity, and extremely small particle sizes with Ag particles well-distributed on the surface. At 2.0% Ag and 1.9% In_2O_3 doping, the Ag/In_2O_3–TiO_2 system exhibited the highest UV-light photocatalytic activity for the degradation of Rhodamine B (RhB) and methyl *tert*-butyl ether (MTBE). In addition, the UV-light photocatalytic activity of three-component systems exceeded that of pure TiO_2 and two-component (Ag/TiO_2 or In_2O_3–TiO_2) systems as well as the commercial P-25 TiO_2. These results indicate that (i) codoped TiO_2 system is more photoactive than single-doped TiO_2 system, (ii) single doped TiO_2 system is more photoactive than pure TiO_2, and (iii) Ag/In_2O_3–TiO_2 with P123 is more photoactive than that prepared without P123. This is explained by (i) enhanced quantum efficiency of Ag and In_2O_3 codoped TiO_2 systems. (ii) Decreased band gap due to coupling of semiconductor In_2O_3 with TiO_2, which results from formation of dopant energy level within the band gap of TiO_2. (iii) Size and morphology of Ag/In_2O_3–TiO_2 are also responsible for its enhanced photocatalytic activity. Chu *et al.*,[91] have synthesized 3D highly porous TiO_2–4%SiO_2–1%TeO_2/Al_2O_3/TiO_2 composite nanostructures (30–120 nm) directly fixed on glass substrates by anodization of a superimposed Al/Ti layer sputter deposited on glass and a sol–gel process. The porous composite nanostructures exhibited enhanced photocatalytic performances in decomposing acetaldehyde gas under UV illumination. Specially, the composite nanostructure showed the highest photocatalytic activity that is 6–10 times higher than commercial P-25 TiO_2.

4. Highly order mesostructured TiO_2–SiO_2 photocatalysts

The mesoporous TiO_2–SiO_2 composites exhibit a binary function for the degradation of organic pollutants derived from their high surface areas and highly crystalline anatase nanoparticles. Large surface areas and pore volumes can enrich organic molecules in the channels in contact with anatase nanocrystals which act as the catalytic sites to degrade the molecules under UV light irradiation. This unique feature enables the composites to exhibit excellent photodegradation activity. Dong *et al.*,[92] have prepared highly ordered 2-D hexagonal mesoporous crystalline TiO_2–SiO_2 nanocomposites with variable Ti/Si ratios (0 to ∞). These mesostructured TiO_2–SiO_2 composites were obtained using TTIP and TEOS as precursors and P123 based on the solvent evaporation-induced co-self-assembly process under a large amount of HCl (Fig. 10).

The amorphous silica acts as a glue linking the TiO_2 nanocrystals and improves the thermal stability. As the silica contents increase, the thermal stability of the resulting mesoporous TiO_2–SiO_2 nanocomposites increases and the size of anatase nanocrystals decreases. The mesoporous TiO_2–SiO_2 nanocomposites exhibit excellent photocatalytic activities more than P25 for the degradation of Rhodamine B in aqueous suspension due to the bifunctional effect of highly crystallized anatase nanoparticles and high porosity (Fig. 11).

Wang *et al.*,[93] have synthesized TiO_2/SBA-15 composites through a postsynthetic approach with the assistance of ethylenediamine. While Li and Zhao,[94] have prepared the same composite for photodecomposition of Orange II. Ethylenediamine plays a double role: (1) etching the surface of silica SBA-15 and directing its regeneration and (2) introducing nitrogen atoms to the lattice of TiO_2. The excellent photocatalytic activity of the composites was evaluated *via* the photodecomposition of phenol in the liquid phase under visible- and ultraviolet-light illumination. The conversion of phenol varies with the content of TiO_2 in the composites, and the optimal value is up to 46.2% under illumination in the visible region. Li and Kim,[95] have prepared a core/shell structure of a nano titania/Ti–O–Si species modified titania embedded in mesoporous silica by the sol–gel method. The as-synthesized TiO_2-$x$$SiO_2$ composites exhibit both much higher absorption capability of organic pollutants and better photocatalytic activity for the photooxidation of benzene than pure titania and P25. The better photocatalytic activity of as-synthesized TiO_2-$x$$SiO_2$ composites than pure titania is attributed to their high surface area, higher UV absorption intensity, and easy diffusion of absorbed pollutants on the absorption sites to photogenerated oxidizing radicals on the photoactive sites. Xuzhuang *et al.*,[96] have fabricated a new composite Ti/clay by reaction between $TiOSO_4$ and a synthetic layered clay laponite. The large number of the anatase crystals

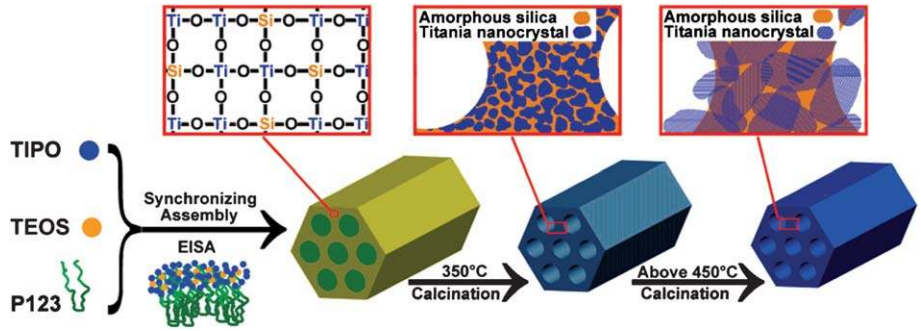

Fig. 10 Scheme for the synchronous assembly of titanate oligomers from TIPO and silicate species from TEOS molecules with triblock copolymer P123 template to form highly ordered mesoporous anatase nanocrystalline TiO_2–SiO_2 composites. Reprinted with permission from ref. 92, Copyright 2007 ACS.

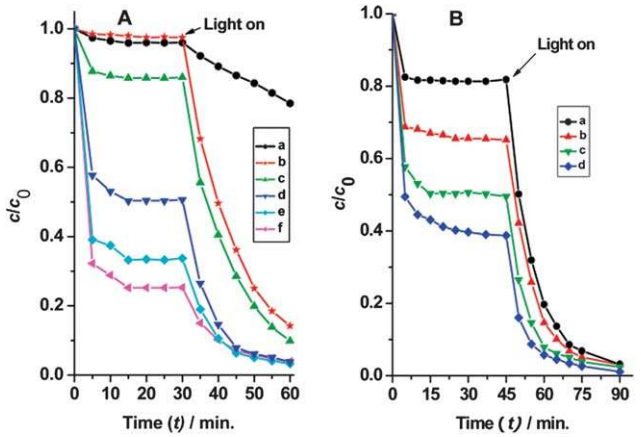

Fig. 11 Photocatalytic degradation of RhB monitored as the normalized concentration change *versus* irradiation time in the presence of (A) mesoporous TiO_2–SiO_2 composites prepared with different Ti/Si ratios. (a) Mesoporous TiO_2 calcined at 400 °C for 2 h; (b) commercial photocatalyst P25; (c) mesoporous $90TiO_2$–$10SiO_2$ composite calcined at 700 °C for 2 h; (d) mesoporous $80TiO_2$–$20SiO_2$, (e) $70TiO_2$–$30SiO_2$, and (f) $60TiO_2$–$40SiO_2$ composites calcined at 850 °C for 2 h. (B) Photocatalytic degradation for mesoporous $80TiO_2$–$20SiO_2$ composites calcined at 700 °C for 4 h (a), 800 °C for 2 h (b), 850 °C for 2 h (c), and 900 °C for 2 h (d). Reprinted with permission from ref. 92, Copyright 2007 ACS.

and better accessibility to the sites by UV light and reactant molecules are the major factors enhancing the photocatalytic activity. The high photocatalytic activity for phenol decomposition resulted from the unique structure of the composite, in which anatase nanocrystals were attached to leached laponite fragments. The performance of the catalysts is related to their structural features, and it is found that the catalytic activity increased with increasing size of the anatase crystals in the catalysts, specific surface area, and mesopore size. Li *et al.*,[97] have synthesized monodispersed concentric hollow nanospheres with mesoporous silica shell and anatase (Fig. 12). Photocatalytic decomposition of methyl orange in the concentric hollow reactors followed an apparent first-order rate law. The observed rate constant for the concentric hollow nanospheres as photocatalysts seems to be lower than those reported for naked and doped TiO_2 nano- and microparticles.[98] The lower reaction rate observed in the present work is probably due to the low content of mesoporous anatase titania in the hollow nanospheres.

Aronson *et al.*,[99] have grafted TiO_2 onto the pore surface of MCM-41 and FSM-16 by reacting $TiCl_4$ in hexanes with the as-synthesized mesostructured silicate. It was found that titania forms well-dispersed isolated $(TiO_2)n$ clusters ($n \approx 30$–70) within the channel structure. These are attached to the silicate walls *via* Si–O–Ti bonds. A minor second phase consisting of anatase crystallites 10–25 nm in diameter on the external surface of the mesoporous silicate crystals was sometimes obtained. It is concluded that an organic moiety, such as the surfactant present in the pores, or a physical constraint, such as the pore walls, is necessary to prevent the creation of large TiO_2 agglomerates and enable the formation of nanosized TiO_2 clusters. The titania-grafted MCM-41 samples exhibited good catalytic activity for photobleaching of Rhodamine-6G and for oxidation of α-terpineol; however, product selectivity was low. Alvaro *et al.*,[100] and Maldotti *et al.*,[101] have reported the preparation of a series of structured mesoporous silicas, starting from colloidal TiO_2 nanoparticles in combination with TEOS using neutral pluronic or cationic CTAB as templates (Fig. 13). Even though the activity of these new mesostructured materials for the degradation of phenol in aqueous solution is lower that those found for P-25 TiO_2, the turnover frequency of the photocatalytic activity is much higher for the mesoporous titania. Also, both pure mesoporous TiO_2 and a mixture of 50% TiO_2 and 50% SiO_2 can induce cyclohexane photooxidation to yield cyclohexanone.

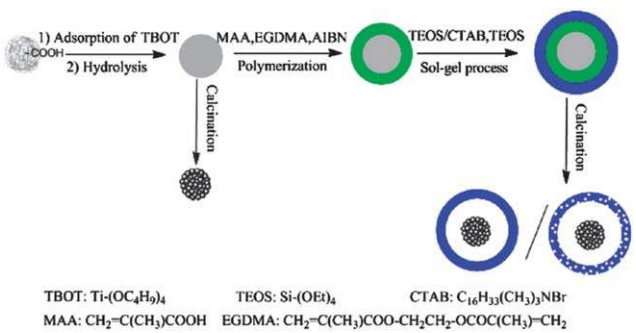

Fig. 12 Schematic of combined polymerization and sol–gel reactions for the preparation of nearly monodispersed concentric hollow nanospheres composed of mesoporous silica shells and anatase titania inner cores. Reprinted with permission from ref. 97, Copyright 2009 ACS.

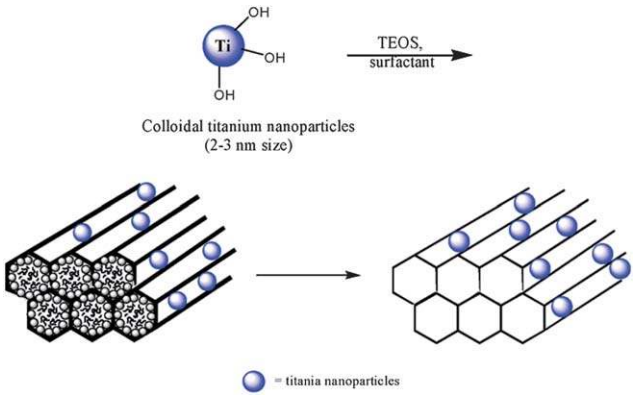

Fig. 13 Schematic of general procedure used for the synthesis of mesoporous materials. Reprinted with permission from ref. 100, Copyright 2006 ACS.

Li *et al.*,[102] have prepared a core/shell SiO_2/TiO_2 photocatalyst using a liquid-phase deposition method. The photocatalytic activity of the core/shell SiO_2/TiO_2 catalyst for the decomposition of Orange II in the liquid phase was observed to be comparable with that of P25. Kang *et al.*,[103] have prepared mesoporous SiO_2-modified nanocrystalline TiO_2 photocatalysts by sol-hydrothermal processes, followed by post-treatment with F127-modified silica sol.[104] Mesoporous SiO_2-modified nanocrystalline TiO_2 samples can exhibit much higher photocatalytic activity for degrading Rhodamine B than P25 TiO_2, which is explained mainly by the high photoinduced charge carrier separation rate resulting from the high anatase crystallinity and the large surface area related to the small nanocrystallite size and mesoporous SiO_2 as well as still possessing a certain amount of surface hydroxyl groups. Hu *et al.*,[105] have prepared Ti-MCM-41 mesoporous molecular sieves using TEOS and TPOT as the starting materials and CTAB as a structure directing agent.[106,107] The photocatalytic reactivity of these catalysts for the decomposition of NO into N_2 and O_2 was found to strongly depend on the local structure of the Ti-oxide species including their coordination and distribution, *i.e.*, the charge transfer excited state of the highly dispersed isolated tetrahedrally coordinated Ti-oxides act as the active sites for the photocatalytic decomposition of NO. Ti-MCM-41 showed higher photocatalytic reactivity than Ti-HMS for the decomposition of NO.

Titania–silica composite films have been fabricated with a high content of crystalline titania phase and periodic mesoporous structure by a low temperature "brick and mortar" approach.[108,109] Pre-formed titania nanocrystals were fused with the surfactant-templated sol–gel silica, which acts as a structure-directing matrix and as a chemical glue (Fig. 14). Using P123 as the structure-directing agent, the structure formation of the mesoporous silica is greatly disturbed as a result of the presence of TiO_2 nanoparticles. On the contrary, the use of F127, whose molecules are larger and whose poly (ethylene oxide) blocks are more hydrophilic, enables the preparation of composite TiO_2–SiO_2 mesoporous architectures that can accommodate up to 50 wt% of nanocrystals and yet retain the periodicity of the porous structure. While films of pure silica are inactive for photooxidation of NO, the activity of those containing TiO_2 nanocrystals increases almost linearly with the TiO_2 content, approaching the conversion efficiency of 3.9–4% for the films composed solely of titania particles taken as a reference. This linearity confirms the homogeneous distribution of the particles and their good accessibility for molecules from the gas phase.

Allain *et al.*,[110] have dispersed colloidal TiO_2 within a transparent silica binder with a mesoporous structure. The TiO_2 particles were then added into the obtained sol by slow addition of a given volume of a commercial aqueous solution of acid-stabilized TiO_2 dispersion.[111] Stearic acid was first deposited on the film by spin-coating from a solution in tetrahydrofuran. Studies of photodegradation kinetics show that such mesoporous films are at least 15 times more active than films synthesized with a usual microporous silica binder. Moreover, the measured quantum-yield efficiency is 1.1% and the improved photoactivity of the films is obtained resulting from the closer proximity between the organic molecules and the surface of the TiO_2 crystallites as well as from the improved diffusion rate of water and oxygen through the interconnected pore network. Ogawa *et al.*,[112] have prepared transparent self-standing films of titanium-containing (Ti/Si ratio of 1/50) silica-surfactant mesostructured materials by the solvent evaporation method from tetramethoxysilane, vinyltrimethoxysilane, TTIP, and octadecyltrimethylammonium chloride. The films were converted to titanium-containing nanoporous silica films by subsequent calcination in air at 550 °C, while their highly ordered mesostructures and macroscopic morphology were retained after the surfactant removal. Titanium-containing nanoporous silica films with hexagonal and cubic symmetry were obtained by changing the composition of the starting mixtures. The titanium ions exist in the silica network as a tetrahedrally coordinated species. UV irradiation of the titanium-containing nanoporous silica film in the presence of CO_2 and H_2O led to the evolution of CH_4 and CH_3OH, indicating high selectivity for the formation of CH_3OH, showing the characteristic reactivity of the charge transfer excited complexes of the tetrahedrally coordinated titanium oxide species.

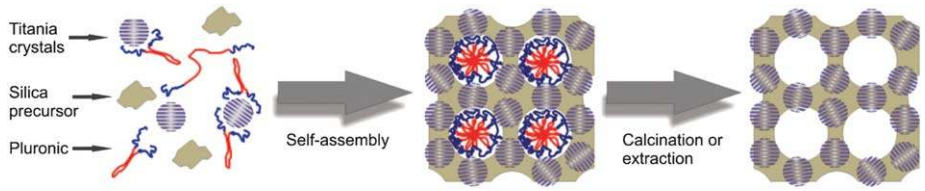

Fig. 14 Formation of nanocomposite titania–silica mesoporous films using pre-formed titania nanocrystals stabilized by the pluronic polymer and amorphous sol–gel silica precursor. Reprinted with permission from ref. 109, Copyright 2009 ACS.

5. Noble metals/mesoporous TiO_2

Doping of noble metals such as Pt, Au, Pd and Ag with mesoporous TiO_2 photocatalysts was proposed to enhance the photocatalytic activity (Table 3) due to their different Fermi levels, characterized by the work function of the metals and the band structure of the semiconductors. Upon contact, a Schottky barrier can be formed between the TiO_2 and the noble metals, leading to a rectified charge carrier transfer.

Ismail *et al.*,[113–117] have synthesized nanocomposites with ordered and disordered mesostructure consisting of noble metals Au, Pt or Pd TiO_2 nanocrystals were prepared through simple one-step sol–gel reactions in the presence of a F127 triblock copolymer as the template to direct the formation of nanostructured photocatalysts. The newly prepared photocatalysts have been compared with commercial photocatalyst Hombikat UV-100 and P 25 by the determination of the rate of HCHO formation generated by the photocatalytic oxidation of CH_3OH and photodegradation of dichloroacetic acid (DCA). This study revealed that ordered and disordered mesostructured noble metals/TiO_2 photocatalysts possess a 2–5 times higher activity for the photooxidation of either CH_3OH or DCA than commercial photocatalysts UV-100 and P 25. Such high photonic efficiencies of the mesoporous noble metals/TiO_2 as compared with Hombikat UV-100 or P 25 can be attributed to several effects, such as a lower light scattering effect of the ordered mesopores, an accumulated local concentration of $^{\cdot}OH$,[118,119] or a fast transport of the target molecules such as CH_3OH or DCA to the active sites due to the facile diffusion of the CH_3OH through the ordered porous network, which for the Hombikat UV-100 reference sample is hindered by the heterogeneities existing in the bulk sample.

Li *et al.*[120] have prepared mesoporous Au/TiO_2 nanocomposites. Briefly, pluronic surfactant P123, $TiCl_4$, $Ti(OBu)_4$, and $AuCl_3$ were mixed in ethanol. Casting the mixture followed by an aging process resulted in homogeneous mesostructured nanocomposites. Calcination removed P123 and created crystalline mesoporous TiO_2 networks embedding gold nanoparticles (Fig. 15). The conversion of phenol oxidation and chromium reduction continuously increases from 22% to 95% when Au content is increased from 0 to 0.5%. A near three-time improvement in phenol decomposition role is achieved when 0.5% of Au was doped, unambiguously suggesting a significantly improved photocatalytic activity.

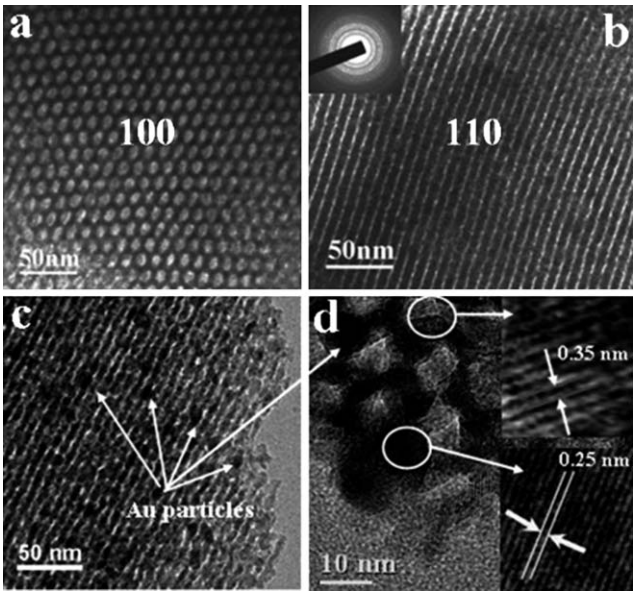

Fig. 15 Representative TEM images of 0.5 mol% Au/TiO_2 along (a) [100] and (b) [110] plane, (c) 1.0 mol% Au/TiO_2 along [110] plane, and (d) high-resolution image of 2.0 mol% Au/TiO_2. Reprinted with permission from ref. 120, Copyright 2007 ACS.

Srinvasn and White,[121] have synthesized 3-D ordered macroporous (3DOM) TiO_2 by colloidal crystal templating against polystyrene spheres using a metal alkoxide precursor. The

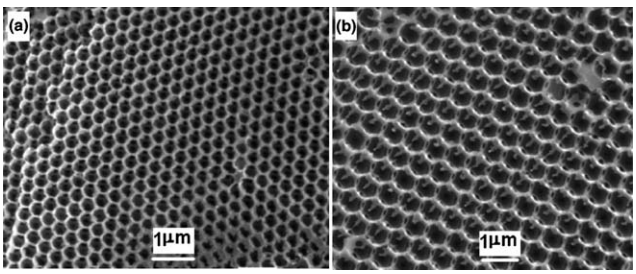

Fig. 16 Secondary electron images (SEI) showing the pore morphology of (a) 0.5 μm (MT5) and (b) 1.0 μm three dimensionally ordered macroporous titania. Reprinted with permission from ref. 121, Copyright 2007 ACS.

Table 3 Textural properties of noble metal nanoparticles (Pt, Au, Pd and Ag) loaded mesoporous TiO_2 and their photocatalytic degradation of organic pollutants from both aqueous and air streams[a]

Noble metals loaded	Template	$P_{S\ TiO2}$/nm	TiO_2 phase	S_{BET}/$m^2\ g^{-1}$	Vp/$cm^3\ g^{-1}$	Dp/nm	Pollutants	Ref.
Pt	P123	6	A	185	0.25	4	*Micrococcus lylae* cells	26
	F127	11	A + R	155	0.24	6	CH_3OH	116
	F127	10	A	150	0.24	6.8	DCA	117
	None	22	A	70		6	CH_3OH	126
Au	F127	5	A	107	0.25	10.8	CH_3OH	113
	P123	12	A				Phenol and Cr^{6+}	120
	F127	10	A	110	0.43	6.5	Soman	124
Pd	F127	10	A	163	0.29	5.8	CH_3OH	114 and 115
Ag	P123	15	A				Stearic acid	25

[a] Soman, (organophosphorus compounds), DCA (dichloroacetic acid), S_{BET} surface area, $P_{S\ TiO2}$ average particle size of TiO_2 nanoparticle, Vp pore volume and Dp pore diameter.

3DOM TiO_2 walls which are predominantly anatase (>98%) were decorated homogeneously with gold nanoparticles (5–7 nm) by pH-controlled precipitation of Au from $HAuCl_4$ using sodium hydroxide. Macroporous 3DOM TiO_2 (Fig. 16) with pore diameter 0.5 μm had the highest first-order rate constant of 0.042 min^{-1} for the decomposition of MB, compared to 0.025 min^{-1} for P25 TiO_2. Deposition of gold on the 3DOM TiO_2 surfaces decreased the reaction rate by covering the surface active sites. For details on Au loaded into porous TiO_2 by different techniques see ref. 24.

Bannat *et al.*,[122] have synthesized mesoporous Au/TiO_2 films by the EISA method. For mesoporous TiO_2 films deposited on an ITO layer, the photonic efficiency for NOx oxidation is higher than for films prepared on glass, because the pore structures are altered. Incorporation of Au results in a significant improvement in the photonic efficiency due to the generation of Schottky barriers, which inhibit the recombination of electron–hole pairs and thereby increase the concentration of photogenerated holes at the film surface reacting with NO. Li *et al.*,[123] have developed a simple method to generate nanoporous organic–inorganic hybrid films and arrays of Au–TiO_2 nanobowls using di-block copolymers as templates in combination with a sol–gel process. The photocatalytic activity of a representative hybrid PS-*b*-PEO–$HAuCl_4$–TiO_2 film in terms of the decomposition of MB is similar in nanostructured TiO_2. Also, mesoporous TiO_2 containing Au NPs has been found to be an efficient photocatalyst for the visible-light decontamination of the chemical warfare agent Soman (organophosphorus compounds).[124] The visible-light photocatalytic activity of mesoporous TiO_2 containing Au NPs towards the deadly Soman is remarkable and it constitutes an environmentally friendly system operating under ambient light at the green atmosphere without the need of corrosive or toxic chemicals.[124]

Silver nanoparticles were introduced into the mesopores using wet impregnation followed by heat treatment.[25,125] Silver nanoparticles were incorporated into the mesoporous titania by *in situ* heat-induced reduction after impregnation of the films in a Ag (I)-containing solution. It was found that the meso-ordered titania had a sufficiently high crystallite content to be photoactive for the oxidation of stearic acid and that the reaction mechanism resembled that of a non-meso-ordered titania sample. It was shown that mesoordered titania was photocatalytically active and that the activity was influenced by the presence of silver nanoparticles. Stathatos *et al.*,[90] reported the synthesis of transparent mesoporous TiO_2 and Ag/TiO_2 films which have been deposited on glass slides by a sol–gel procedure in the presence of Triton X-100 reverse micelles in cyclohexane. Basic Blue 41 has been adsorbed on these films and the photodegradation of the dye by visible-light illumination has been monitored by absorption spectrophotometry. Films doped with silver ions are more efficient photocatalysts than pure titanium films and become even more efficient when they are treated with UV radiation. Films doped with ruthenium ions are less efficient for photocatalysis but when they are treated with UV radiation, they also become more efficient photocatalysts than pure titania films.[90]

Wang *et al.*,[26] have prepared highly dispersed Pt nanoparticles embedded in a cubic mesoporous anatase thin film. The diameter of the Pt cluster can be controlled to be below 5 nm, and the high dispersion of these clusters gives rise to catalytic activity for the oxidation of CO. Furthermore, the pore-stabilized Pt particles contact and interact with the anatase–TiO_2 nanocrystals embedded in the mesonetwork, forming semiconductor/metal nanoheterojunctions. These nanoheterojunctions promote the separation of charge carriers on UV-excited TiO_2, thus significantly improving the photocatalytic activity of porous Pt/TiO_2 composites toward killing bacteria cells of *M. lylae*. Lakshminarasimhan *et al.*,[126] have synthesized mesoporous TiO_2 consisting of compactly packed nanoparticles without surfactant. The activity of meso-TiO_2 exhibited a unique dependence on Pt cocatalyst loading. Under both UV and visible light irradiation, the highest activity for H_2 production was obtained around 0.1 wt% Pt and further increase reduced the activity, whereas other nonporous TiO_2 samples exhibited a typical saturation behavior with increasing Pt load. The enhanced photocatalytic activity of meso-TiO_2 is ascribed to the compact and dense packing of TiO_2 nanoparticles forming a uniform agglomerate, which enables efficient charge separation through interparticle charge transfer.

In general, the suggested mechanism of noble metals/mesoporous TiO_2 for photooxidation of methanol has been illustrated (Fig. 17). 3-D mesoporous TiO_2 network acts as an antenna system transferring the initially generated electrons from the location of light absorption to a suitable interface with the noble metal catalyst and subsequently to the location of the noble metal nanoparticle where the actual electron transfer reaction will take place. Within this antenna model, it can be envisaged that the overlap of the energy bands of the nanoparticles forming this network will result in unified energy bands for the entire system enabling a quasi-free movement of the photogenerated charge carriers throughout. Consequently, an electron generated by light absorption within one of the nanoparticles forming the network will subsequently be available to promote redox processes anywhere within the structure. Assuming a Schottky contact between the mesoporous titanium dioxide network and the noble metal particle, the noble metal particles then serve as active sites for the reduction of molecular oxygen, on which the trapped photogenerated electrons are transferred to oxygen producing $O_2^{\bullet-}$ radicals. It should be noted

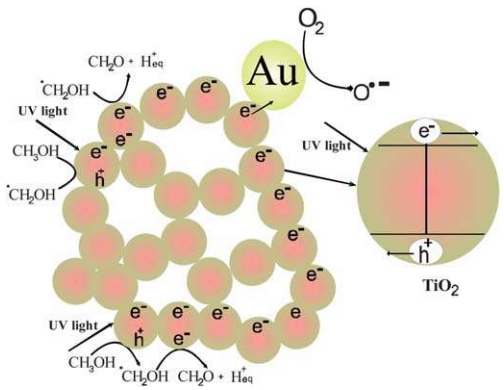

Fig. 17 Schematic illustration of the proposed antenna mechanism to explain the enhanced activity for methanol photooxidation over mesoporous Au/TiO_2 nanocrystals as photocatalysts. Reprinted with permission from ref. 113, Copyright 2009 ACS.

that it is frequently overseen that this latter process is really the "bottle-neck" in most photocatalytic transformations being the rate-determining step due to its very small thermodynamic driving force. Thus its acceleration through the electron transfer catalysis induced by the Au deposits will result in the observed increase in the yield of the photocatalytic methanol oxidation.[113–117]

6. Nonmetal doped/mesoporous TiO_2 photocatalysts

One of the endeavors to improve the performance of TiO_2 is to increase its optical activity by shifting the onset of its response from the UV to the visible region. A promising approach is the doping of TiO_2 with nonmetals such nitrogen, carbon and fluoride and iodine. The rationale behind this approach is to sensitize TiO_2 toward visible light either by generating newly created midgap states or by narrowing the band gap. The observed band gap shift from the UV into the visible region has been attributed to (i) substitution of lattice oxygen by the anion or (ii) formation of interstitial species in vacancies or micro-voids that give rise to surface or near-surface states.[127–129] The effects of doping nonmetals into mesoporous TiO_2 for degradation of different pollutants such as MB,[131,134,135,144,145] acetone[18,147,148] RhB[132,139,141] and chlorophenol (CP)[19,132,143] are summarized in Table 4.

6.1. Nitrogen doped TiO_2 mesoporous

Fang *et al.*,[130] have prepared visible-light-active mesoporous N-doped TiO_2 photocatalysts by the precipitation of the titanyl oxalate complex ($[TiO(C_2O_4)_2]_2^-$). N–TiO_2 photocatalysts exhibit comparable UV-light activity and visible-light activity in the photodegradation of methyl orange. The doped N species locates the interstitial sites in TiO_2, which leads to the band gap narrowing of TiO_2. A novel and interesting result is that N-doped TiO_2 calcined at 400 °C has Bronsted acid sites arising from covalently bonded dicarboxyl groups, which greatly enhances the adsorption capacity for methyl orange. Chi *et al.*,[131] prepared mesoporous N-doped TiO_2 microspheres employing a template-free solvothermal method. The N-doped TiO_2 mesoporous spheres show higher visible-light photocatalytic activity than the undoped TiO_2 (Fig. 18). The dual role of urea helps the formation of a mesoporous structure and the doping of nitrogen into TiO_2 to be completed simultaneously during the solvothermal process. The amount of urea shows a crucial effect on the mesoporous structure and nitrogen doping in TiO_2. The enhanced photocatalytic activities of N–TiO_2 in UV light may be due to the increase of the surface deficiency after the introduction of nitrogen into the TiO_2 structure. It also could be found that, with the increase of the nitrogen amount in the spheres, the visible-light photocatalytic activity was also be enhanced, which could be the evidence to confirm the role of nitrogen in the lattice for improvement of the visible-light response of N–TiO_2.

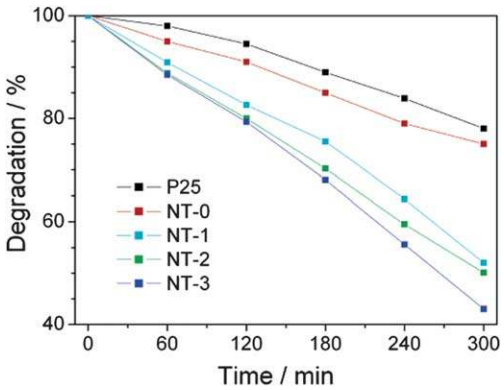

Fig. 18 Photocatalytic activities of NT mesoporous spheres and Degussa P25 under visible-light irradiation ($\lambda > 420$ nm) for degradation MB. The molar ratio of urea to $Ti(OBu)_4$ was adjusted as 0, 1, 2, and 3. Reprinted with permission from ref. 130, Copyright 2007 ACS.

Table 4 Synthesis routes and textural properties of mesoporous non-metals doping TiO_2 nanoparticles and their photocatalytic degradation of organic pollutants from both aqueous and air streams[a]

Synthesis routes	Non-metal ions	Template	$P_{S\ TiO2}$/nm	TiO_2 phase	S_{BET}/$m^2\ g^{-1}$	Vp/$cm^3\ g^{-1}$	Dp/nm	Pollutants	Ref.
Sol–gel	N	DDAM	10	A	150	0.202	4.5	MC-LR	17
		None	10	A	85	0.117	4.4	MO	130
		None	6	A	220		3.5	Ethylene	133
		P123		A				MB	134
		F127	11 ± 2	A			9	MB	135
Solvothermal		None	7–8	A	154	0.466	6.6	MB	131
Hydrothermal		None	8.4	A				CP and RhB	132
Sol–gel	F	None		A + R + B	76.5	0.21	9.2	Acetone	18
		P123		A	70	0.088	5	Acetone	148
Hydrothermal		None			21.6		10	MB	144
		None	8	A				MB	145
		None	10	A		0.19	6	Acetone	147
Sol–gel	C	None	20	A + R	22.4		8.5	NO	16
		F127	6.4	A	191	0.19	4.1	RhB	139
		None	5	A + R	334	0.19		RhB	141
Hydrothermal		None		A	29	0.1	15	CP	143
Hydrothermal	I	None	10	A				CP	19

[a] Methyl orange (MO), methylene blue (MB), microcystin-LR (MC-LR), Rhodamine B (RhB), chlorophenol(CP), dodecylammonium chloride (DDAM), particle size D, anatase (A), rutile (R), brookite (B), S_{BET} surface area, $P_{S\ TiO2}$ average particle size of TiO_2 nanoparticle, Vp pore volume and Dp pore diameter.

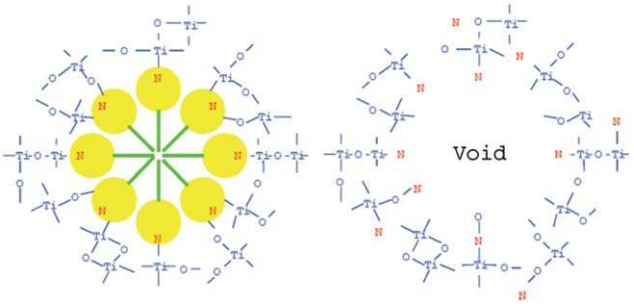

Fig. 19 Schematic incorporation of Ti–O–Ti network onto self-organized DDAC surfactant micelles to form an organic core/inorganic shell composite, followed by the removal of the organic templates to form N–TiO_2 with mesoporous structure. Reprinted with permission from ref. 17, Copyright 2007 ACS.

Nitrogen-containing surfactant dodecylammonium chloride (DDAC) was introduced as a pore templating material for tailor-designing the structural properties of TiO_2 and as a nitrogen dopant for its visible light response (Fig. 19).[17] Red shift in light absorbance up to 468 nm, 0.9 eV lower binding energy of electrons in Ti 2p state, and reduced interplanar distance of crystal lattices proved nitrogen doping in the TiO_2 lattice. Due to its narrow band gap at 2.65 eV, N–TiO_2 efficiently degraded the cyanobacterial Toxin Microcystin-LR (MC-LR) under visible illumination above 420 nm. Acidic conditions (pH 3.5) were more favorable for the adsorption and photocatalytic degradation of MC-LR on N–TiO_2 due to electrostatic attraction forces between negatively charged MC-LR and charged N–TiO_2. Even under UV light, MC-LR was decomposed 3–4 times faster using N–TiO_2 than control TiO_2. The degradation pathways and reaction intermediates of MC-LR were not directly related to the energy source for TiO_2 activation (UV and visible) and nature of TiO_2.

Cong *et al.*,[132] have synthesized N-doped TiO_2 nanocatalysts with a homogeneous anatase structure through a microemulsion-hydrothermal method by using triethylamine, urea, thiourea, and hydrazine hydrate. In the microemulsion system, Triton X-100 was used as the surfactant, 1-hexanol as the cosurfactant, cyclohexane as the continuous oil phase, and TBOT dissolved in nitric acid as the aqueous phase. XPS analysis indicated that nitrogen was doped effectively and most nitrogen dopants might be present in the chemical environment of Ti–O–N and O–Ti–N. The results of the photodegradation of Rhodamine B and 2,4-CP upon the visible light irradiation ($\lambda > 420$ nm) suggested that the TiO_2 photocatalysts after nitrogen doping were greatly improved compared with the undoped TiO_2 photocatalysts and Degussa P-25. Wang *et al.*,[133] have prepared mesoporous $TiO_{2-x}N_x/ZrO_2$ visible-light photocatalysts by sol–gel method. Results revealed that nitrogen was doped into the lattice of TiO_2 by the thermal treatment of NH_3-adsorbed TiO_2 hydrous gels, converting the TiO_2 into a visible-light responsive catalyst. The photocatalytic activity of the samples was evaluated by the decomposition of ethylene in air under visible light ($\lambda > 450$ nm) illumination. The activity of the $TiO_{2-x}N_x$ is initially quite high and decreases rapidly with increasing calcination temperature. At the sintering temperature of 400 °C, the conversion of C_2H_4 on $TiO_{2-x}N_x$ is 28%, but it drops to 7% at 500 °C. Soni *et al.*,[134] have prepared N-doped TiO_2 mesoporous thin films templated using titanium alkoxide solution containing thiourea as the nitrogen source and P123 by EISA method. The shift in the band gap was monitored by UV-vis spectroscopy and the photocatalytic properties were characterized by monitoring the photodegradation of MB upon irradiation with visible light. Multiply coated thin films having different thicknesses were prepared to improve the efficiency of N-doped TiO_2 thin films. The adsorption capacity and photocatalytic activity of thin films in the visible region were bigger for multiply coated films than for thinner films as a result of their increased surface area. Martínez-Ferrero reported the preparation nanocrystalline mesoporous N-doped TiO_2.[135] Briefly, the initial solution, containing $TiCl_4$/EtOH/H_2O/F127 with molar ratios of 1 : 40 : 10 : 0.005, was stirred for 15 min at room temperature for homogenization.[136,137] The introduction of nitrogen into the anatase structure starts at 500 °C, with N bonding to titanium *via* oxygen substitution. Microstructural characterization shows that the ordered mesoporosity is maintained until 700 °C, where TiN ($TiN_{1-x}O_x$) begins to form. The photocatalytic tests for degradation of MB give the best results under visible light excitation for the film nitride at 500 °C. At this temperature the concentration of nitrogen in the structure is optimal since oxygen vacancies are still not important enough to promote the recombination of the photogenerated electrons and holes. Nitrogen doping could inhibit the recombination of the photoinduced electron and thereafter increase the efficiency of the photocurrent carrier.

6.2. Carbon doped mesoporous TiO_2

Huang *et al.*,[16] have prepared mesoporous nanocrystalline C-doped TiO_2 photocatalysts through a direct solution phase carbonization using $TiCl_4$ and diethanolamine as precursors. XPS analysis revealed that oxygen sites in the TiO_2 lattice were substituted by carbon atoms and formed a C–Ti–O–C structure. The samples showed a more effective removal efficiency of NO than TiO_2 P25. However, for the C-doped TiO_2 calcined at 500 °C, the removal rate reached the highest value after being irradiated for 30 min. Comparing with the C-doped TiO_2 calcined at 600 °C, the carbon-doped TiO_2 calcined at 500 °C showed superior photocatalytic activity for the degradation of NO at parts per billion levels, which can be explained by the band gap energy, the surface properties, as well as the mesoporous architecture. According to the above mechanism, inhibiting the undesirable electron–hole pair recombination is important to enhance the photocatalytic activity because it can improve the ability to produce hydroxyl radical group ·OH, which is possibly beneficial for oxidation of NO. A recent study revealed that the holes formed for carbon-doped TiO_2 photocatalysts under visible light irradiation were less reactive than those formed under UV light irradiation for pure TiO_2.[136] For the carbon-doped TiO_2 samples, the holes were trapped at midgap levels and showed less mobility, which was beneficial for the capture of surface hydroxyl to produce ·OH. However, the density and nature of the localized states in the band gap were significantly influenced by the carbon dopant concentration,[138] which may be used to explain the difference in photocatalytic activity of carbon-doped TiO_2 calcined at 500 and 600 °C on the degradation of NO at typical parts per billion levels. Liu *et al.*,[139] have

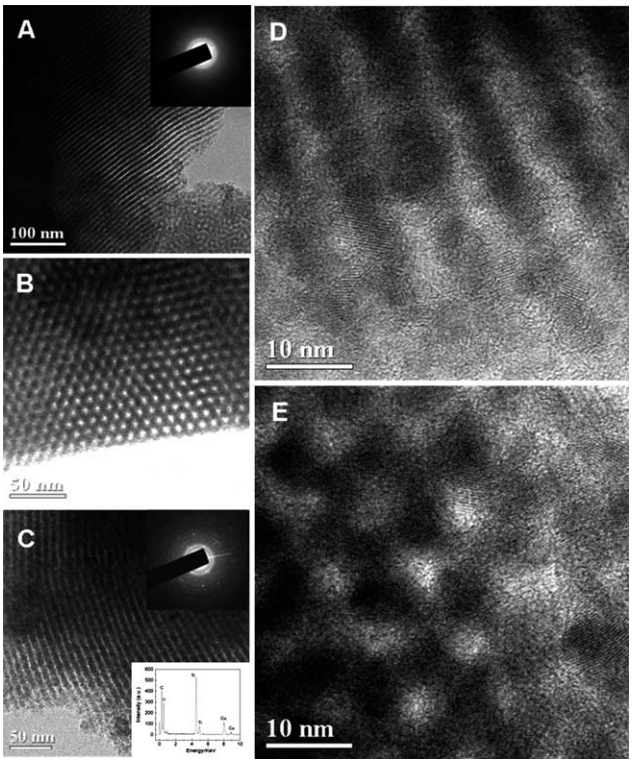

Fig. 20 (A–C) TEM images, (D and E) HRTEM image of mesoporous carbon–titania nanocomposites (30C-70TiO_2-450 and 30C-70TiO_2-600) calcined at 450 (A and B) and 600 °C (C–E), viewed from the [110] (A, C and D) and [001] (B and E) directions. Insets are the SAED patterns and EDX analysis taken at the same area. Reprinted with permission from ref. 139, Copyright 2008 ACS.

reported highly ordered mesoporous carbon–titania nanocomposites with nanocrystal-glass frameworks *via* the organic–inorganic–amphiphilic coassembly followed by the *in situ* crystallization technology (Fig. 20). In typical synthesis, the carbon–titania nanocomposites were synthesized *via* the evaporation-induced triconstituent co-assembly followed by the *in situ* crystallization technology. The resol precursor ($M_w < 500$) used as a carbon precursor was prepared accordingly.[140] The carbon–titania nanocomposites with controllable texture properties and composition can be obtained in a wide range from 20 to 80 wt% TiO_2 by adjusting the initial mass ratios. The C–TiO_2 nanocomposites with "bricked-mortar" frameworks exhibit highly ordered 2D hexagonal mesostructure and high thermal stability up to 700 °C. The nanocomposites have high surface area (465 $m^2\ g^{-1}$) and large pore size (~4.1 nm). The carbon–titania nanocomposites show good photocatalytic activity for the photodegradation of Rhodamine B in an aqueous suspension, which may be attributed to the highly crystallized frameworks and high adsorptive capacity from the large surface areas.

Zhang *et al.*,[141] have prepared hollow TiO_2 microparticles about 20–60 μm in size and hollow TiO_2/carbon composite microparticles about 30–90 μm in size by employing commercial Sephadex G-100 beads as the template as well as the carbon precursor. The photocatalytic activity of the obtained hollow microparticles of TiO_2 and TiO_2/carbon composites was investigated by monitoring the photodegradation of Rhodamine B. Compared with the hollow TiO_2 microparticles, the hollow TiO_2/carbon composite microparticles exhibit remarkably enhanced photocatalytic activity. Lei *et al.*,[142] prepared a 3D ordered macroporous TiO_2/graphitized carbon. The graphitized carbons were formed by catalytic graphitization of polystyrene arrays, which were used as both template and carbon source for the generation of the macroporous composite. It was found that the TiO_2/graphitized carbon showed higher activity in terms of degradation of Rhodamine B and eosin Y than TiO_2/amorphous carbon and TiO_2 P25. Also, TiO_2@C core–shell composite nanoparticles were synthesized by a simple and efficient single-step method in a specially made Swagelok cell at different temperatures.[143] It is evident from TEM analysis that the as-prepared samples are core–shell structures of TiO_2, anatase phase, and C. The prepared samples were tested for their photochemical activities for 4-chlorophenol degradation. The sample prepared at 700 °C showed comparable activity for the degradation of 4-chlorophenol with that of Degussa P25. The photobleaching studies of methylene blue were also carried out under sunlight. It was found that the TiO_2@C samples showed higher photocatalytic activity than Degussa P25.

6.3. Fluoride doped mesoporous TiO_2

Pan *et al.*,[144] have synthesized monodisperse F–TiO_2 hollow microspheres by hydrothermal treatment of TiF_4 in H_2SO_4 aqueous solution at 160 °C for 4 h. The removal rates of MB over the course of the photocatalytic degradation reaction indicates that with identical UV-light exposure of 6 h, the mesoporous F–TiO_2 hollow microspheres show higher photocatalytic activity in the degradation of MB than that of P25. F^- ions doped into crystalline TiO_2 by hydrothermal treatment of TiF_4 in an HCl solution have been synthesized.[145,146] FE-SEM and TEM images showed that the products exhibited a flowerlike morphology with a hollow interior. The flowerlike F-doped TiO_2 hollow microspheres showed the highest photocatalytic activity for the degradation of MB under visible light irradiation. Yu *et al.*,[18] have used a novel and simple method for preparing highly photoactive nanocrystalline F-doped TiO_2 photocatalyst with anatase and the brookite phase by hydrolysis of TTIP in a mixed NH_4F–H_2O solution. F^- ions not only suppressed the formation of brookite phase but also prevented phase transition of anatase to rutile. The photocatalytic activity for oxidation of acetone in air by F-doped TiO_2 photocatalysts exceeded that of Degussa P25 when the molar ratio of NH_4F to H_2O was kept in the range of 0.5–3.

Yu *et al.*,[147] have prepared mesoporous surface-fluorinated TiO_2 anatase phase by a one-step hydrothermal strategy in a NH_4HF_2–H_2O–C_2H_5OH mixed solution with TBOT as precursor. The photocatalytic activity of F–TiO_2 powders for decomposition of acetone is obviously higher than that of pure TiO_2 and P25 by a factor of more than 3 times due to the fact that the strong electron-withdrawing ability of the surface Ti–F groups reduces the recombination rate of photogenerated electrons and holes, and enhances the formation of free ·OH radicals. Yu *et al.*,[148] prepared TiO_2 thin films using TTIP in the presence of a P123. The surface modification of the films was conducted by dipping the as prepared TiO_2 films in an aqueous

trifluoroacetic acid (TFA) solution at room temperature. The photocatalytic activity of modified TiO_2 thin films for acetone oxidation in air is higher than that of unmodified TiO_2 thin films, and the modified film treated at 250 °C shows the highest activity. This is ascribed to the fact that the TFA complex bound on the surface of TiO_2 acts as an electron scavenger and, thus, reduces the recombination of photogenerated electrons and holes. The enhancement is only temporary, however, as the TFA eventually decomposes under the strong oxidizing environment of photocatalysis.

6.4. Iodine doped mesoporous TiO_2

Cheng *et al.*[149] have synthesized iodine-doped mesoporous TiO_2 without a template by the hydrothermal method. I-doped mesoporous TiO_2 (MTI) with a bicrystalline framework exhibits higher visible light activity for the photodegradation of methylene blue than the I-doped TiO_2 (TI) with anatase structure. The disordered mesoporous structure is beneficial for promoting the diffusion of reactants and products, enhancing the photocatalytic activity by facilitating the access to the reactive sites on the surface of the photocatalyst. The high absorbance from 400 to 550 nm for samples MTI and TI was attributed to iodine doping. However, to obtain high photocatalytic activity, it is vital to decrease the combination probability of the photoinduced electron–hole pairs in the photocatalyst. The superiority of MTI to TI is attributed to the bicrystalline framework, large surface area, high crystallinity and mesoporous structure. With these characteristics of the sample MTI, the separation of photoinduced electron hole pairs is favorable. Tojo *et al.*,[19] have prepared iodine-doped TiO_2 powders (I–TiO_2) *via* hydrothermal treatment. A higher photodegradation efficiency of 4-chlorophenol (4-CP) was observed for I–TiO_2 under UV- and visible-light irradiation, when compared to the undoped TiO_2 (Fig. 21).

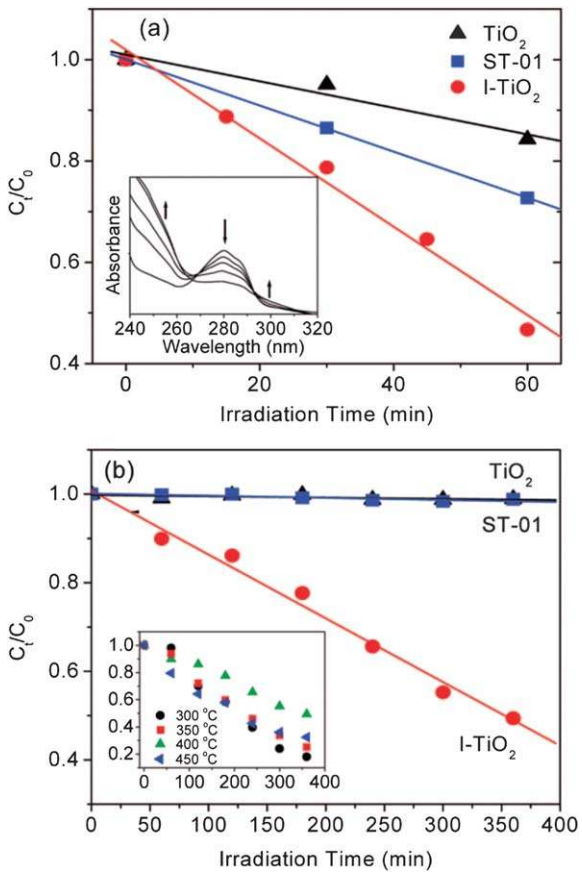

Fig. 21 Comparison of the photocatalytic decomposition of 4-CP in the presence of TiO_2 (triangles), I–TiO_2 (circles), and commercial anatase TiO_2 (ST-01, Ishihara Sangyo) ST-01 (squares) as monitored by the changes in absorbance at 280 nm after UV- (a) and visible-light (>440 nm) (b) irradiation. C_0 indicates the initial concentration of 4-CP. The inset in panel (a) shows the UV-light irradiation time dependence of absorption spectra of 4-CP obtained for I–TiO_2. The inset in panel (b) shows the effect of calcined temperature on the photodegradation of 4-CP obtained for I–TiO_2. Reprinted with permission from ref. 19, Copyright 2008 ACS.

Mechanism of I–TiO_2 photocatalytic reaction. To date, it has been shown that nonmetal cationic doping is a feasible strategy for developing highly efficient UV- and visible-light responsive photocatalysts (Fig. 22). However, the photocatalytic activity decreased with the increasing amount of dopants, such as N atoms, in TiO_2 since the doping sites (and/or defect sites) could serve as charge recombination centers. On the other hand, in the case of I–TiO_2, the recombination of e^-–h^+ pairs is sufficiently inhibited because the doping I sites act as trapping site to capture the e^-. Recently, Cai *et al.* have carried out the first principle calculations on I–TiO_2. They proposed that I 5p and/or I 5s orbitals mixed with O 2p and Ti 3d orbitals contribute to the valence and conduction bands, respectively.[150] It is very difficult to directly detect the migration (trapping) processes of the photogenerated charge carriers, especially, hot carriers, in I–TiO_2, has been proposed assuming a possible mechanism that the continuous states consisting of 5p and/or 5s orbitals of I^{5+} and O 2p orbitals of the valence band are favorable for efficient trapping of h^+ at the I-induced states (Fig. 22). It is inferred that a large amount of h^+ generated in I–TiO_2 is localized in the particle (not at the surface). Tojo *et al.*,[151] concluded that photocatalytic reactions of organic compounds on N-, S-, and C-doped TiO_2 under visible-light irradiation proceeds *via* reactions with surface intermediates of reactive oxygen species (ROS), such as $O_2^{\cdot-}$, $OH^{\cdot}$, and $^1O_2$.[151,152] Fu *et al.* reported that the photogenerated h^+ left in the valence band of I–TiO_2 oxidizes OH^- to give $OH^{\cdot}$ under visible-light illumination.[153] However, such mechanism is implausible because of the low E_{ox} of

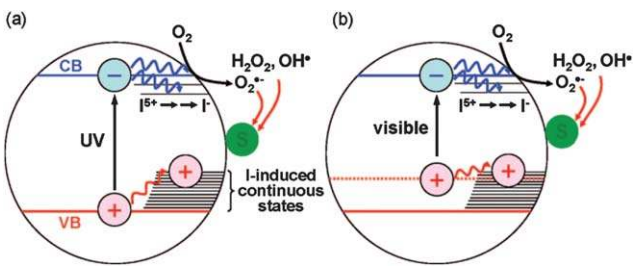

Fig. 22 Schematic illustrations of the I–TiO_2 photocatalytic reaction processes under UV- (a) and visible-light (b) irradiation. Reprinted with permission from ref. 19, Copyright 2008 ACS.

trapped h^+, compared with that of OH^- (E_{ox}) +1.9 V *vs* NHE).[154] Therefore, it is considered that the photocatalytic reactions of I–TiO_2 proceed *via* indirect oxidation processes with OH, which is probably generated from the electron transfer from trapped e^- to adsorbed H_2O_2.[155]

7. Summary and outlook

The review strategy has been focused on the synthesis of mesoporous TiO_2, doped transition metals, precious metals, or nonmetals. Besides the synthetic methods, architecture concepts, and their photocatalytic activities under UV and visible light have been highlighted. The direct synthesis of mesoporous materials with a crystalline wall has been considered to be difficult for several reasons. One major reason is that phase transformation from amorphous to crystalline by heat treatment or UV light irradiation usually induces the collapse of mesopores because the wall is too thin to retain the 3DM structure during crystallization. Mesoporous TiO_2 prepared by sol–gel reaction using surfactant lyotropic liquid crystals as the reaction template has gathered considerable interest as one of the best techniques. However, the wall of these materials is normally amorphous, and under heat treatment, crystallization results in collapse of the uniform mesoporous structure. Shabata *et al.*, have succeeded to synthesize highly ordered mesoporous TiO_2 with crystalline walls by sol–gel methods.[40] Also, hydrothermal treatment is considered as the most efficient method to prepare disordered mesostructured TiO_2.

The development of synthesis methods for various mesoporous materials based on TiO_2 allows further enhancement of the photocatalytic performance of TiO_2. The reason of high photocatalytic activity of mesoporous TiO_2 is explained by, (i) the larger specific surface area of mesoporous TiO_2 *versus* Degussa P25 powder; hence, there are more reactant adsorption/desorption sites for catalytic reaction. (ii) the prevention of the unwanted aggregation of the nanoparticles clusters, which is also helpful in maintaining the high active surface area. (iii) the highly porous structure, which allows rapid diffusion of various pollutants during the reaction. (iv) the smaller crystal size, which means more powerful redox ability owing to the quantum-size effect; moreover, the smaller crystal sizes are also beneficial for the separation of the photogenerated hole and electron pairs.

The photocatalytic oxidation using either highly ordered hexagonal TiO_2 networks in samples calcined at 350 °C, catalysts with randomly ordered mesoporous channels after calcinations at 450 °C or disordered mesostructures prepared at 550 °C are comparable although the crystallinity of the TiO_2 nanoparticles increases strongly only with calcination temperatures exceeding 500 °C. This indicates that good charge carrier transport properties are as well important as high crystallinity of the anatase phase. The results indicate that a highly ordered mesoporous system is not a prerequisite for high photocatalytic activity.

References

1 C. T. Kresge, M. E. Leonowicz, W. J. Roth, J. C. Vartuli and J. S. Beck, *Nature*, 1992, **359**, 710–712.
2 S. A. Davis, S. L. Burkett, N. H. Mendelson and S. Mann, *Nature*, 1997, **385**, 420–423.
3 W.-S. Chae, S.-W. Lee and Y.-R. Kim, *Chem. Mater.*, 2005, **17**, 3072–3074.
4 P. Yang, D. Zhao, D. I. Margolese, B. F. Chmelka and G. D. Stucky, *Nature*, 1998, **396**, 152.
5 D. M. Antonelli and J. Y. Ying, *Angew. Chem., Int. Ed. Engl.*, 1995, **34**, 2014–2017.
6 D. Li, H. Zhou and I. Honma, *Nat. Mater.*, 2004, **3**, 65–72.
7 J. Orilall, M. C. Warrwn, S. C. Kamperman, M. Disalvo and F. J. U. Wiesner, *Nat. Mater.*, 2008, **7**, 222–228.
8 M. Niederberger, M. H. Bartl and G. D. Stucky, *Chem. Mater.*, 2002, **14**, 4364–4370.
9 G. Goutailler, C. Guillard, S. Daniele and L. G. Hubert-Pfalzgraf, *J. Mater. Chem.*, 2003, **13**, 342–346.
10 D.-W. Lee, S.-K. Ihm and K.-H. Lee, *Chem. Mater.*, 2005, **17**, 4461–4467.
11 Y. Li and S.-J. Kim, *J. Phys. Chem. B*, 2005, **109**, 12309–12315.
12 S. Chappel, S. Chen and A. Zaban, *Langmuir*, 2002, **18**, 3336–3342.
13 S. Takeuchi, T. Katayama, T. Sugiyama, M. Matsuda, M. Kitamura, T. Wada and Y. S. Yanagida, *Chem. Mater.*, 2003, **15**, 2824–2828.
14 A. A. Ismail and D. W. Bahnemann, *ChemSusChem*, 2010, **3**, 1057–1062.
15 K. Nagaveni, G. Sivalingam, M. S. Hegde and G. Madras, *Appl. Catal., B*, 2004, **48**, 83–93.
16 Y. Huang, W. Ho, S. Lee, L. Li, G. Zhang and J. C. Yu, *Langmuir*, 2008, **24**, 3510–3516.
17 H. Choi, M. G. Aantoniou, M. Pelaez, A. A. Delacruz, O. A. Shoemaker and D. D. Dionysiou, *Environ. Sci. Technol.*, 2007, **41**, 7530–7535.
18 J. C. Yu, J. G. Yu, W. K. Ho, Z. T. Jiang and L. Z. Zhang, *Chem. Mater.*, 2002, **14**, 3808–3816.
19 S. Tojo, T. Tachikawa, M. Fujitsuka and T. Majima, *J. Phys. Chem. C*, 2008, **112**, 14948–14954.
20 A. K. Sinha and K. Suzuki, *J. Phys. Chem. B*, 2005, **109**, 1708–1714.
21 J. H. Schattka, D. Shchukin, G. Jia, J. M. Antonietti and R. A. Caruso, *Chem. Mater.*, 2002, **14**, 5103–5108.
22 R. J. Tayade, R. G. Kulkarni and R. V. Jasra, *Ind. Eng. Chem. Res.*, 2006, **45**, 5231–5238.
23 D. Jing, Y. Zhang and L. Guo, *Chem. Phys. Lett.*, 2005, **415**, 74.
24 X. Wang and R. A. Caruso, *J. Mater. Chem.*, 2011, **21**, 20–28.
25 M. Andersson, H. Birkedal, N. R. Franklin, T. Ostomel, S. Boettcher, A. C. Palmqvist and G. D. Stucky, *Chem. Mater.*, 2005, **17**, 1409–1415.
26 X. Wang, J. C. Yu, H. Y. Yip, L. Wu, P. K. Wong and S. Y. Lai, *Chem.–Eur. J.*, 2005, **11**, 2997–3004.
27 L. Chen, B. Yao, Y. Cao and K. Fan, *J. Phys. Chem. C*, 2007, **111**, 11849–11853.
28 V. Kalousek, J. Tschirch, D. Bahnemann and J. Rathousky, *Superlattices Microstruct.*, 2008, **44**, 506–513.
29 E. Beyers, P. Cool and E. F. Vansant, *J. Phys. Chem. B*, 2005, **109**, 10081–10086.
30 H. Wang, J.-J. Miao, J.-M. Zhu, H.-M. Ma, J.-J. Zhu and H.-Y. Chen, *Langmuir*, 2004, **20**, 11738–11747.
31 A.-C. Lee, R.-H. Lin, C.-Y. Yang, M.-H. Lin and W.-Y. Wang, *Mater. Chem. Phys.*, 2008, **109**, 275–280.
32 M. Wark, J. Tschirch, O. Bartels, D. Bahnemann and J. Rathousky, *Microporous Mesoporous Mater.*, 2005, **84**, 247–253.
33 Y. Shiraishi, N. Saito and T. Hirai, *J. Am. Chem. Soc.*, 2005, **127**, 12820–12822.
34 B. Tian, H. Yang, X. Liu, S. Xie, C. Yu, J. Fan, B. Tu and D. Zhao, *Chem. Commun.*, 2002, 1824–1825.
35 Y. Liu, J. Li, M. Wang, Z. Li, H. Liu, P. He, X. Yang and J. Li, *Cryst. Growth Des.*, 2005, **5**, 1643.
36 Y. Lu, M. R. Hoffmann, S. Yelamanchili, A. Terrenoire, M. Schrinner, M. Drechsler, M. W. Moller, J. Breu and M. Ballauff, *Macromol. Chem. Phys.*, 2009, **210**, 377–386.
37 S. Zhan, D. Chen, X. Jiao and C. Tao, *J. Phys. Chem. B*, 2006, **110**, 11199–11204.
38 S. Madhugiri, B. Sun, P. G. Smirniotis, J. P. Feraris and K. J. Balkus, Jr, *Microporous Mesoporous Mater.*, 2004, **69**, 77–83.
39 J. Yu, W. H. Liu and A. Yu, *Cryst. Growth Des.*, 2008, **8**, 930–934.
40 H. Shibata, T. Ogura, T. Mukai, T. Ohkubo, H. Sakai and M. Abe, *J. Am. Chem. Soc.*, 2005, **127**, 16396–16397.
41 T. Sugimoto and X. P. Zhou, *J. Colloid Interface Sci.*, 2002, **252**, 347.

42 J. Liu, T. An, G. Li, N. Bao, G. Fu and J. Sheng, *Microporous Mesoporous Mater.*, 2009, **124**, 197–203.
43 G. J. Soler-Illia, A. A. de Louis and A. C. Sanchez, *Chem. Mater.*, 2002, **14**, 750–759.
44 J. Patarin, B. Lebeau and R. Zana, *Curr. Opin. Colloid Interface Sci.*, 2002, **7**, 107–115.
45 J. Yu, L. Zhang, B. Cheng and Y. Su, *J. Phys. Chem. C*, 2007, **111**, 10582–10589.
46 H. Xu and L. Zhang, *J. Phys. Chem. C*, 2009, **113**, 1785–1790.
47 G. Tian, H. Fu, L. Jing, B. Xin and K. Pan, *J. Phys. Chem. C*, 2008, **112**, 3083–3089.
48 T. Peng, D. Zhao, K. Dai, W. Shi and K. Hirao, *J. Phys. Chem. B*, 2005, **109**, 4947–4952.
49 X. C. Wang, J. C. Yu, C. M. Ho, Y. D. Hou and X. Z. Fu, *Langmuir*, 2005, **21**, 2552.
50 Z. Liu, D. D. Sun, P. Guo and J. O. Leckie, *Chem.–Eur. J.*, 2007, **13**, 1851–1855.
51 D. S. Kim and S.-Y. Kwak, *Appl. Catal., A*, 2007, **323**, 110–118.
52 H.-W. Wang, C.-H. Kuo, H.-C. Lin, I.-T. Kuo and C.-F. Cheng, *J. Am. Ceram. Soc.*, 2006, **89**, 3388–3392.
53 J. C. Yu, L. Zhang and J. Yu, *Chem. Mater.*, 2002, **14**, 4647–4653.
54 J. Yu, M. Zhou, B. Cheng, H. Yu and X. Zhao, *J. Mol. Catal. A: Chem.*, 2005, **227**, 75–80.
55 K. Wessels, M. Minnermann, J. Rathousky, M. Wark and T. Oekermann, *J. Phys. Chem. C*, 2008, **112**, 15122–15128.
56 Y. Matsumoto, Y. Ishikawa, M. Nishida and S. Ii, *J. Phys. Chem. B*, 2000, **104**, 4204–4209.
57 H. Choi, A. C. Sofranko and D. D. Dionysiou, *Adv. Funct. Mater.*, 2006, **16**, 1067–1074.
58 X. Wang, J. C. Yu, Y. Hou and X. Fu, *Adv. Mater.*, 2005, **17**(1), 99–102.
59 K. Wang, B. Yao, M. A. Morris and J. D. Holmes, *Chem. Mater.*, 2005, **17**, 4825–4831.
60 D. S. Kim and S.-Y. Kwak, *Environ. Sci. Technol.*, 2009, **43**, 148–151.
61 M. R. Hoffmann, S. T. Martin, W. Y. Choi and D. W. Bahnemann, *Chem. Rev.*, 1995, **95**, 69.
62 H. Vidal, J. Kapar, M. Pijolat, G. Colon, S. Bernal, A. Cordon, V. Perrichon and F. Fally, *Appl. Catal., B*, 2001, **30**, 75.
63 J. Georgieva, S. Armyanov, E. Valova, I. Poulios and S. Sotiropoulos, *Electrochem. Commun.*, 2007, **9**, 365.
64 S. Xuan, W. Jiang, X. Gong, Y. Hu and Z. Chen, *J. Phys. Chem. C*, 2009, **113**, 553–558.
65 T. W. Kim, H.-W. Ha, M.-J. Paek, S.-H. Hyun, I.-H. Baek, J.-H. Choy and S.-J. Hwang, *J. Phys. Chem. C*, 2008, **112**, 14853–14862.
66 J. Zhu, J. Ren, Y. Huo, Z. Bian and H. Li, *J. Phys. Chem. C*, 2007, **111**, 18965–18969.
67 P. Arnal, R. J. P. Corriu, D. Leclercq, P. H. Mutin and A. Vioux, *J. Mater. Chem.*, 1996, **6**, 1925–1932.
68 K. Mori, Y. Kondo, S. Morimoto and H. Yamashita, *J. Phys. Chem. C*, 2008, **112**, 397–404.
69 W. Zhou, H. Fu, K. Pan, C. Tian, Y. Qu, P. Lu and C.-C. Sun, *J. Phys. Chem. C*, 2008, **112**, 19584–19589.
70 Z. Bian, J. Zhu, S. Wang, Y. Cao, X. Qian and H. Li, *J. Phys. Chem. C*, 2008, **112**, 6258–6262.
71 L. Kong, H. Chen, W. Hua, S. Zhang and J. Chen, *Chem. Commun.*, 2008, 4977–4979.
72 X. Zhang, L. Zhang, T. Xie and D. Wang, *J. Phys. Chem. C*, 2009, **113**, 7371–7378.
73 J. C. Yu, G. Li, X. Wang, X. Hu, C. W. Leung and Z. Zhang, *Chem. Commun.*, 2006, 2717–2719.
74 X. Fan, X. Chen, S. Zhu, Z. Li, T. Yu, J. Ye and Z. Zou, *J. Mol. Catal. A: Chem.*, 2008, **284**, 155–160.
75 D. R. Rolison, *Science*, 2003, **299**, 1698.
76 A. T. Bell, *Science*, 2003, **299**, 1688.
77 J. C. Yu, X. C. Wang and X. Z. Fu, *Chem. Mater.*, 2004, **16**, 1523–1530.
78 S. Rodrigues, K. T. Ranjit, S. Uma, I. N. Martyanov and K. J. Klabunde, *Adv. Mater.*, 2005, **17**, 2467–2471.
79 V. Houskova, V. Stengl, S. Bakardjieva, N. Murafa and V. Tyrpekl, *Appl. Catal., B*, 2009, **89**, 613–619.
80 A. A. Ismail, L. Robben and D. W. Bahnemann, *ChemPhysChem*, 2011, **12**, 982–991.
81 J. H. Pan and W. I. Lee, *Chem. Mater.*, 2006, **18**, 847–853.
82 S. Liu, J. Yu and S. Mann, *J. Phys. Chem. C*, 2009, **113**, 10712–10717.
83 R. Nakamura, A. Okamoto, H. Osawa, H. Irie and K. Hashimoto, *J. Am. Chem. Soc.*, 2007, **129**, 9596–9597.
84 T. W. Kim, S.-J. Hwang, Y. Park, W. Choi and J.-H. Choy, *J. Phys. Chem. C*, 2007, **111**, 1658–1664.
85 V. F. Stone and R. J. Davis, *Chem. Mater.*, 1998, **10**, 1468–1474.
86 J. C. Yu, L. Zhang, Z. Zheng and J. Zhao, *Chem. Mater.*, 2003, **15**, 2280–2286.
87 K. Dai, T. Peng, H. Chen, J. Liu and L. Zan, *Environ. Sci. Technol.*, 2009, **43**, 1540–1545.
88 T. Peng, D. Zhao, H. B. Song and C. H. Yan, *J. Mol. Catal. A: Chem.*, 2005, **238**, 119–126.
89 X. Yang, Y. Wang, L. Xu, X. Yu and Y. Guo, *J. Phys. Chem. C*, 2008, **112**, 11481–11489.
90 E. Stathatos, T. Petrova and P. Lianos, *Langmuir*, 2001, **17**, 5025–5030.
91 S.-Z. Chu, S. Inoue, K. Li, D. Wada, H. Haneda and S. Awatsu, *J. Phys. Chem. B*, 2003, **107**, 6586–6589.
92 W. Dong, Y. Sun, C. W. Lee, W. Hua, X. Lu, Y. Shi, S. Zhang, J. Chen and D. Zhao, *J. Am. Chem. Soc.*, 2007, **129**, 13894–13904.
93 Z. Wang, F. Zhang, Y. Xue, B. Cui and J. N. Guan, *Chem. Mater.*, 2007, **19**, 3286–3293.
94 G. Li and X. S. Zhao, *Ind. Eng. Chem. Res.*, 2006, **45**, 3569–3573.
95 Y. Li and S.-J. Kim, *J. Phys. Chem. B*, 2005, **109**, 12309–12315.
96 Y. Xuzhuang, D. Yang, Z. Huaiyong, L. Jiangwen, W. N. Martins, R. Frost, L. Daniel and S. Yuenian, *J. Phys. Chem. C*, 2009, **113**, 8243–8248.
97 G. Li, E. T. Kang, K. G. Neoh and X. Yang, *Langmuir*, 2009, **25**, 4361–4364.
98 X. H. Wang, J. G. Li, H. Kamiyama, Y. Moriyoshi and T. Ishigaki, *J. Phys. Chem. B*, 2006, **110**, 6804–6809.
99 B. J. Aronson, C. F. Blanford and A. Stein, *Chem. Mater.*, 1997, **9**, 2842–2851.
100 M. Alvaro, C. Aprile, M. Benitez, E. Carbonell and H. Garcıa, *J. Phys. Chem. B*, 2006, **110**, 6661–6665.
101 A. Maldotti, A. Molinari, R. Amadelli, E. Carbonell and H. Garcia, *Photochem. Photobiol. Sci.*, 2008, **7**, 819–825.
102 G. Li, R. Bai and X. S. Zhao, *Ind. Eng. Chem. Res.*, 2008, **47**, 8228–8232.
103 C. Kang, L. Jing, T. Guo, H. Cui, J. Zhou and H. Fu, *J. Phys. Chem. C*, 2009, **113**, 1006–1013.
104 K. Y. Shi, Y. J. Chi, H. T. Yu and H. G. Fu, *J. Phys. Chem. B*, 2005, **109**, 2546–2551.
105 Y. Hu, G. Martra, J. Zhang, S. Higashimoto, S. Coluccia and M. Anpo, *J. Phys. Chem. B*, 2006, **110**, 1680–1685.
106 W. Zhang, M. Froba, J. Wang, P. T. Tanev, J. Wong and T. J. Pinnavaia, *J. Am. Chem. Soc.*, 1996, **118**, 9164–9171.
107 A. Thangaraj, R. Kumar, S. P. Mirajkar and P. Ratnasamy, *J. Catal.*, 1991, **130**, 1–8.
108 J. M. Szeifert, D. F. Rohlfing, D. Georgiadou, V. Kalousek, J. Rathouský, D. Kuang, S. Wenger, S. M. Zakeeruddin, M. Grätzel and T. Bein, *Chem. Mater.*, 2009, **21**, 1260–1265.
109 D. F. Rohlfing, J. Szeifert, M. Q. Yu, V. Kalousek, J. Rathousky and T. Bein, *Chem. Mater.*, 2009, **21**, 2410–2417.
110 E. Allain, S. Besson, C. Durand, M. Moreau, T. Gacoin and J.-P. Boilot, *Adv. Funct. Mater.*, 2007, **17**, 549–554.
111 S. Besson, C. Ricolleau, T. Gacoin, C. Jacquiod and J.-P. Boilot, *Microporous Mesoporous Mater.*, 2003, **60**, 43–49.
112 M. Ogawa, K. Ikeue and M. Anpo, *Chem. Mater.*, 2001, **13**, 2900–2904.
113 A. A. Ismail, D. W. Bahnemann, I. Bannat and M. Wark, *J. Phys. Chem. C*, 2009, **113**, 7429–7435.
114 A. A. Ismail, D. W. Bahnemann, L. Robben and M. Wark, *Chem. Mater.*, 2010, **22**, 108–116.
115 A. A. Ismail, T. A. Kandiel and D. W. Bahnemann, *J. Photochem. Photobiol., A*, 2010, **216**, 183–193.
116 A. A. Ismail and D. W. Bahnemann, *Green Chem.*, 2011, **12**, 428–435.
117 A. A. Ismail and D. W. Bahnemann, *J. Phys. Chem. C*, 2011, **115**, 5784–5791.
118 D. Lawless, N. Serpone and D. Meisel, *J. Phys. Chem.*, 1991, **95**, 5166–5170.
119 S. Tojo, T. Tachikawa, M. Fujitsuka and T. Majim, *Chem. Phys. Lett.*, 2004, **384**, 312–316.

120 H. Li, Z. Bian, J. Zhu, Y. Huo, H. Li and Y. Lu, *J. Am. Chem. Soc.*, 2007, **129**, 4538–4539.
121 M. Srinvasn and T. White, *Environ. Sci. Technol.*, 2007, **41**, 4405–4409.
122 I. Bannat, K. Wessels, T. Oekermann, J. Rathousky, D. Bahnemann and M. Wark, *Chem. Mater.*, 2009, **21**, 1645–1653.
123 X. Li, J. Peng, J.-H. Kang, J.-H. Choy, M. Steinhart, W. Knoll and D. H. Kim, *Soft Matter*, 2008, **4**, 515–521.
124 M. Alvaro, B. Cojocaru, A. A. Ismail, N. Petrea, B. Ferrer, F. A. Harraz, V. I. Parvulescu and H. Garcia, *Appl. Catal., B*, 2010, **99**, 191–197.
125 P. C. A. Alberius, K. L. Frindell, R. C. Hayward, E. J. Kramer, G. D. Stucky and B. F. Chmelka, *Chem. Mater.*, 2002, **14**, 3284–3294.
126 N. Lakshminarasimhan, E. Bae and W. Choi, *J. Phys. Chem. C*, 2007, **111**, 15244–15250.
127 R. Asahi, T. Morikawa, T. Ohwaki, K. Aoki and Y. Taga, *Science*, 2001, **293**, 269.
128 H. Irie, Y. Wanatabe and K. Hashimoto, *J. Phys. Chem. B*, 2003, **107**, 5483.
129 C. Burda, Y. Lou, X. Chen, A. C. S. Samia, J. Stout and J. L. Gole, *Nano Lett.*, 2003, **3**, 1049.
130 J. Fang, F. Wang, K. Qian, H. Bao, Z. Jiang and W. Huang, *J. Phys. Chem. C*, 2008, **112**, 18150–18156.
131 B. Chi, L. Zhao and T. Jin, *J. Phys. Chem. C*, 2007, **111**, 6189–6193.
132 Y. Cong, J. Zhang, F. Chen and M. Anpo, *J. Phys. Chem. C*, 2007, **111**, 6976–6982.
133 X. Wang, J. C. Yu, Y. Chen, L. Wu and X. Fu, *Environ. Sci. Technol.*, 2006, **40**, 2369–2374.
134 S. S. Soni, M. J. Henderson, J.-F. Bardeau and A. Gibaud, *Adv. Mater.*, 2008, **20**, 1493–1498.
135 E. Martínez-Ferrero, Y. Sakatani, C. Boissière, D. Grosso, A. Fuertes, J. Fraxedas and C. Sanchez, *Adv. Funct. Mater.*, 2007, **17**, 3348–3354.
136 D. Grosso, F. G. Cagnol, A. A. Soler-Illia, E. L. Crepaldi, H. Amenitsch, A. Brunet-Bruneau, A. Bourgeois and C. Sanchez, *Adv. Funct. Mater.*, 2004, **14**, 309.
137 D. G. Grosso, A. A. Soler-Illia, E. L. F. Crepaldi, F. Cagnol, A. Bourgeois, A. Brunet-Bruneau, H. Amenitsch, P. A. Albouy and C. Sanchez, *Chem. Mater.*, 2003, **15**, 4562.
138 C. Di Valentin, G. Pacchioni and A. Selloni, *Chem. Mater.*, 2005, **17**, 6656.
139 R. Liu, Y. Ren, Y. Shi, F. Zhang, L. Zhang, B. Tu and D. Zhao, *Chem. Mater.*, 2008, **20**, 1140–1146.
140 Y. Meng, D. Gu, F. Q. Zhang, Y. F. Shi, H. Yang, F. Li, Z. Yu, C. Z. Tu and B. D. Y. Zhao, *Angew. Chem., Int. Ed.*, 2005, **44**, 7053.
141 D. Zhang, D. Yang, H. Zhang, C. Lu and L. Qi, *Chem. Mater.*, 2006, **18**, 3477–3485.
142 Z. Lei, Y. Xiao, L. Dang, G. Hu and J. Zhang, *Chem. Mater.*, 2007, **19**, 477–484.
143 S. Shanmugam, A. Gabashvili, D. S. Jacob, J. C. Yu and A. Gedanken, *Chem. Mater.*, 2006, **18**, 2275–2282.
144 J. H. Pan, X. Zhang, A. J. Du, D. D. Sun and J. O. Leckie, *J. Am. Chem. Soc.*, 2008, **130**, 11256–11257.
145 J. K. Zhou, L. Lv, J. Yu, H. L. Li, P.-Z. Guo, H. Sun and X. S. Zhao, *J. Phys. Chem. C*, 2008, **112**, 5316–5321.
146 H. G. Yang and H. C. Zeng, *J. Phys. Chem. B*, 2004, **108**, 3492–3495.
147 J. Yu, W. Wang, B. Cheng and B.-L. Su, *J. Phys. Chem. C*, 2009, **113**, 6743–6750.
148 J. C. Yu, W. Ho, J. Yu, S. K. Hark and K. Iu, *Langmuir*, 2003, **19**, 3889–3896.
149 G. Liu, Z. Chen, C. Dong, Y. Zhao, F. Li, G. Q. Lu and H.-M. Cheng, *J. Phys. Chem. B*, 2006, **110**, 20823–20828.
150 M. Long, W. Cai, Z. Wang and G. Liu, *Chem. Phys. Lett.*, 2006, **420**, 71–76.
151 T. Tachikawa, S. Tojo, K. Kawai, M. Endo, M. Fujitsuka, T. Ohno, K. Nishijima, Z. Miyamoto and T. Majima, *J. Phys. Chem. B*, 2004, **108**, 19299–19306.
152 T. Tachikawa, Y. Takai, S. Tojo, M. Fujitsuka, H. Irie, K. Hashimoto and T. Majima, *J. Phys. Chem. B*, 2006, **110**, 13158–13165.
153 W. Su, Y. Zhang, Z. Li, L. Wu, X. Wang, J. Li and X. Fu, *Langmuir*, 2008, **24**, 3422.
154 P. Wardman, *J. Phys. Chem. Ref. Data*, 1989, **18**, 1637.
155 T. Hirakawa, K. Yawata and Y. Nosaka, *Appl. Catal., A*, 2007, **325**, 105–111.